Licensing Technical Report

NuScale Comprehensive Vibration Assessment Program Analysis Technical Report

December 2022

Revision 0

Docket: 52-050

NuScale Power, LLC
1100 NE Circle Blvd., Suite 200
Corvallis, Oregon 97330
www.nuscalepower.com

© Copyright 2022 by NuScale Power, LLC

Licensing Technical Report

COPYRIGHT NOTICE

This report has been prepared by NuScale Power, LLC and bears a NuScale Power, LLC, copyright notice. No right to disclose, use, or copy any of the information in this report, other than by the U.S. Nuclear Regulatory Commission (NRC), is authorized without the express, written permission of NuScale Power, LLC.

The NRC is permitted to make the number of copies of the information contained in this report that is necessary for its internal use in connection with generic and plant-specific reviews and approvals, as well as the issuance, denial, amendment, transfer, renewal, modification, suspension, revocation, or violation of a license, permit, order, or regulation subject to the requirements of 10 CFR 2.390 regarding restrictions on public disclosure to the extent such information has been identified as proprietary by NuScale Power, LLC, copyright protection notwithstanding. Regarding nonproprietary versions of these reports, the NRC is permitted to make the number of copies necessary for public viewing in appropriate docket files in public document rooms in Washington, DC, and elsewhere as may be required by NRC regulations. Copies made by the NRC must include this copyright notice and contain the proprietary marking if the original was identified as proprietary.

Licensing Technical Report

Department of Energy Acknowledgement and Disclaimer

This material is based upon work supported by the Department of Energy under Award Number DE-NE0008928.

Table of Contents

Table of Contents

List of Tables

List of Figures

List of Figures

Abstract

This report describes the Comprehensive Vibration Assessment Program (CVAP) for the NuScale Power Module (NPM) that verifies the structural integrity of the internals for flow-induced vibration. The CVAP conforms to the guidance of Regulatory Guide 1.20, Revision 4. The content of this licensing technical report provides additional information to substantiate the statements made in the NuScale Power Plant US460 standard design, thereby facilitating a comprehensive review by the NRC of the NPM-20 design.

Executive Summary

A Comprehensive Vibration Assessment Program (CVAP) for the NuScale Power Module (NPM) is established in accordance with Regulatory Guide 1.20, Revision 4. The CVAP ensures that the components of the NPM exposed to fluid flow do not experience the detrimental effects of flow-induced vibration (FIV).

The NPM-20 represents a first-of-a-kind design in its size, arrangement, and operating conditions. Accordingly, the first operational NPM-20 is classified as a prototype in accordance with Regulatory Guide 1.20. The terms NPM-20 and NPM are used interchangeably throughout this report. After the first NPM-20 is qualified as a valid prototype, subsequent NPMs are classified as non-prototype.

Given its prototype classification, the CVAP addresses the applicable criteria of Regulatory Guide 1.20, Section C.2.

The NPM is a small modular reactor that is an integral, movable nuclear steam supply system. The NPM design is passive, with primary coolant driven by natural circulation flow. Low natural circulation flow velocities decrease the propensity for detrimental FIV effects. The CVAP establishes the scope of analyses, testing, measurements, and inspections required to ensure that components of the NPM are not subject to unacceptable vibratory degradation. When completed, the CVAP provides the requisite assurance that the NPM components are not subject to detrimental effects of FIV.

1.0 Introduction

1.1 Purpose and Scope

This report describes the Comprehensive Vibration Assessment Program (CVAP) analysis program for the NuScale Power Module (NPM)-20 to verify the structural integrity of the components subject to flow-induced vibration (FIV). The terms NPM-20 and NPM are used interchangeably throughout this report. The CVAP conforms to the guidance of Regulatory Guide 1.20 Revision 4 and demonstrates a sufficient margin of safety and structural integrity through:

- design vibration and stress analysis
- testing to quantitatively validate analytical methods and results
- inspection prior to and following initial startup testing to qualitatively validate analytical methods and results

In defining the scope of the CVAP, the U.S. Nuclear Regulatory Commission (NRC) references the definition of reactor core support and internal structures inside the reactor pressure vessel (RPV) defined by the Boiler and Pressure Vessel Code (BPVC), Section III, Division 1, Subsection NG, of the American Society of Mechanical Engineers (ASME) (Reference 8.27). The NuScale reactor vessel internals (RVI) and the steam generator (SG) tube supports are designed to Subsection NG; however, the pressure boundary components of the NuScale SG (i.e., tubes, plenums) are designed to Section III, Division 1, Subsection NB.

Based on the integral design of the NPM, the SG pressure-containing components are located within the fluid volume of the RPV, along with the reactor internal components. Likewise, Regulatory Guide 1.20 includes references to evaluation of steam dryers, steam system components, and SG internal components as part of a CVAP. Regulatory Guide 1.20 does not discuss the need to evaluate the vibration characteristics of the fuel components, which include both the fuel bundles and the control rod assemblies (CRAs). Based on these considerations, there are three focus areas within the NPM that are included within the scope of the CVAP: reactor vessel internals and structures, steam generator components, and the NPM piping up to and including the NPM disconnect flanges.

To finalize the CVAP, two additional technical reports are developed. The first report (Reference 8.13) contains details on the measurement program and inspection requirements. Upon completion of validation testing and inspection, the second report provides the post-test evaluation and inspection program results. In this second report, the differences between the expected and measured experimental results are either resolved or confirmed to be in the analytically predicted allowable ranges.

1.2 Abbreviations

Table 1-1 Abbreviations

Term	Definition
AR	acoustic resonance
ASME	American Society of Mechanical Engineers
CFD	computational fluid dynamics
CNTS	containment system
CNV	containment vessel
CRA	control rod assembly
CRAGT	control rod assembly guide tube
CRD	control rod drive
CVAP	Comprehensive Vibration Assessment Program
CVCS	chemical and volume control system
DHRS	decay heat removal system
DWO	density wave oscillations
FEI	fluid elastic instability
F/G	flutter/gallop
FIV	flow-induced vibration
FW	feedwater
GT	guide tube
ICIGT	in-core instrument guide tube
IFR	inlet flow restrictor
ISP	integral steam plenum
LFI	leakage flow instability
MS	main steam
MSIV	main steam isolation valve
NPM	NuScale Power Module
PSD	power spectral density
PWR	pressurized water reactor
RCS	reactor coolant system
RG	Regulatory Guide
RMS	root mean square
RPV	reactor pressure vessel
RRV	reactor recirculation valve
RVI	reactor vessel internals
RVV	reactor vent valve
RXC	reactor core
SG	steam generator
SGS	steam generator system
SONGS	San Onofre Nuclear Generator Station
TB	turbulent buffeting
TH	thermal-hydraulic
URS	upper riser shell
VS	vortex shedding

Table 1-2 Definitions

Term	Definition
Acoustic resonance	A phenomenon where an acoustic wave is generated at a frequency that coincides with the natural frequency of a confining structure.
Initial startup testing	Testing conducted on the prototype after fuel loading.
Fixed boundary condition	For the “fixed” boundary condition, bonded contacts are used to simulate the situation that tubes are fixed to support channels. This boundary condition simulates high frictional forces between the tubes and tubes supports.
Fluid elastic instability	Instability that arises when, during one vibration cycle, the energy absorbed from the fluid exceeds the energy dissipated by damping. This phenomenon is associated with arrays of closely packed circular cylinders.
Flutter/gallop	The phenomenon in which drag and lift forces due to fluid flow act on a bluff body with a non-circular cross section. If the bluff body vibrates, the draft and lift forces change due to the change in flow angle, which can increase the vibration amplitude. In this phenomenon, the amount of energy dissipated by damping is less than the energy imparted on the structure by the fluid flow.
Leakage flow instability	A condition in which fluid flow through a thin space with at least one flexible structural boundary results in vibration of the flexible boundary due to the negative fluid damping becoming larger than the total fluid damping.
Prototype	A configuration of RVI that, because of its arrangement, design, size, or operating conditions, represents a unique design for which no valid example exists.
Prototype testing	Testing that is used to validate analysis inputs, methods, and margins of safety for components susceptible to FIV phenomena. This testing consists of separate effects and initial startup testing. Testing is required to be performed using a full-scale, prototypic arrangement of the region of interest. Separate effects testing is performed at a test facility. Initial startup testing is performed on the first NPM after fuel loading.
Safety margin	For strongly-coupled FIV mechanisms, the percentage difference between the analytically predicted value and the acceptance criteria that represent the predicted onset of the mechanism for a component. For turbulent buffeting, safety margins are evaluated for the analytically-predicted fatigue against the limits that are acceptable over the component design life.
Separate effects testing	Testing performed on a prototypic portion of the NPM in a test facility.
Sliding boundary condition	For the “sliding” boundary condition, no separation contacts are used to simulate the situation that tubes can slide in the support channels. This boundary condition models no frictional forces between the tube and the tube support.
Turbulent buffeting	A weak coupling between a structure and the random pressure fluctuations induced by turbulent flow. The effects of low amplitude structural vibrations induced from turbulence are evaluated to assess impact and fatigue.
Valid prototype	A configuration of RVI that successfully completed a comprehensive vibration assessment program for prototype RVI and experienced no adverse in-service vibration phenomena.
Vortex shedding	A phenomenon due to flow separation on the surface of a bluff body located in the flow field, leading to the shedding of vortices at locations of flow separation. Due to interaction between the vortices, time varying forces are generated that act on the body.

2.0 NuScale Power Module Design Overview for Flow-Induced Vibration

The NPM is an integral, movable nuclear steam supply system, as described in the Final Safety Analysis Report (FSAR) Section 1.2, General Plant Description. The NPM includes the containment system (CNTS), the reactor coolant system (RCS), the control rod drive system, the reactor core (RXC), the steam generator system (SGS), the in-core instrumentation system, the decay heat removal system (DHRS), and the emergency core cooling system. The outer NPM vessel is the containment vessel (CNV). An integral RPV, which includes the pressurizer and the SGs, is located inside the CNV.

Figure 2-1 Nuscale Power Module General Arrangement

{{

}}2(a),(c),ECI

2.1 Primary Coolant Flow Conditions

The RCS is a passive system driven by natural circulation flow that relies on interfacing active systems for operational control. During operation at power, the reactor coolant circulates inside the RPV.

Reactor coolant flows upward through the Reactor Core (RXC) where it removes heat from the fuel assemblies. The heated reactor coolant exits the RXC and continues to flow upward through the central riser (composed of the lower and upper riser assemblies). At the top of the upper riser, the flow is turned by the pressurizer baffle plate to flow downward through the annular space between the upper riser and the RPV. This annular space between the upper riser and the RPV contains the SG helical tube bundles. As the reactor coolant flows downward across the SG tube bundles, it transfers heat to the SGs and is cooled. The colder reactor coolant leaving the SG helical tube bundles continues to flow downward through the annular space between the core barrel and the RPV. As flow passes the bottom of the core barrel, the flow is turned upward by the RPV lower head and flow diverter, and is returned to the RXC. The motive force for the reactor coolant flow during operation at power is natural circulation, driven by the difference in coolant density between the hot coolant leaving the RXC and the colder coolant leaving the SGs, and the elevation difference between the RXC (heat source) and the SGs (heat sink).

The NPM reactor coolant flow has the following operational characteristics:

- There are no RCS pumps. Primary coolant flow is by natural circulation. Flow is limited by thermal driving head, with no pump overspeed conditions, no excess flow in transients, and no modulating pressure excitation due to vane passing frequencies.
- Primary and secondary flows are mostly axial, with no RPV hot and cold leg nozzles impinging flow on the core support assembly. The low-velocity axial flows result in low turbulent sources for FIV.
- Primary single-phase flow is on the outside of the SG tubes with low velocity. Flow velocity is approximately an order of magnitude less than pressurized water reactor (PWR) designs with secondary-side two-phase flow on the inside of tubes.

A schematic of the primary coolant flow path is shown in FSAR Section 1.2. Table 2-1 summarizes the maximum design reactor coolant flows in relation to other PWR applications. In the SG tube region, only a simplified depiction of the flow is provided. The primary-side flow occurs in the downward direction, across the columns of helical SG tubes. The secondary-side flow travels in the upward direction inside the helical SG tubes. The RCS water level is normally maintained in the pressurizer region above the elevation of the pressurizer heaters. The water in the pressurizer region is heated by the pressurizer to maintain a saturated water-steam interface in the pressurizer region.

Table 2-1 Pressurized Water Reactor Flow Velocity Comparison

Design (Note 1)	Average Velocity (ft/s)				Maximum Design Flow Rate (lb_m/s)	Primary Coolant Loop Transit Time (seconds)
	Steam Generator Gap	Downcomer	Core	Upper Internals Cross Flow		
NuScale	{{ }}2(a),(c),ECI	{{ }}2(a),(c),ECI	3.5	{{ }}2(a),(c),ECI	1735	80.0
EPR		24	16	30	55,000	9.9
AP1000		19	16	40	34,400	10.3
US-APWR		23	14	30	54,092	12.6
SONGS	18	-	-	-	-	-

Notes: (1) Velocities, maximum design flow rates, and loop transit times for the EPR, US-APWR and AP1000 PWR designs are per Reference 8.5, Reference 8.6, Reference 8.7, and Reference 8.8.
(2) SONGS steam generator gap velocity is per Reference 8.9.

2.2 Secondary Coolant Flow Conditions

During normal operations, feedwater is supplied to the SGS from the condensate and feedwater system (CFWS) via the CNTS feedwater lines and steam is routed from the SGS to the main steam system (MSS) via the CNTS steam lines. The SGs are once through helical coils with primary side reactor coolant outside of the tubes and secondary-side fluid inside of the tubes. Each SG has a pair of feedwater plenums and a pair of steam plenums. Preheated feedwater enters the SGS feedwater piping from the CNTS feedwater lines and then enters the SGs via the feedwater supply nozzles and feedwater plenums. Feedwater flows up the helical tubes where it is heated, boiled, and superheated before it exits the SGs via the steam plenum and main steam supply nozzles to the SGS steam lines.

The SG tube inlet flow restrictor provides secondary side pressure drop for flow stability. Secondary side steady-state parameters are controlled as a function of reactor power and the highest flow rates occur at full-power conditions. The steam piping velocity at full-power operating conditions is below {{ }}2(a),(c),ECI feet per second.

Following DHRS actuation, the SGS is isolated from the CFWS and MSS and forms a closed loop with the DHRS. Feedwater is then supplied to the SGS via the DHRS condensate lines and steam is routed from the SGS to the DHRS steam lines (via the CNTS steam lines). The DHRS condensate lines connect to the SGS feedwater lines at a cross fitting inside containment.

2.3 Component Screening for Flow-Induced Vibration

Table 2-2 provides a summary of the NPM components screened for susceptibility to FIV. The following subsections discuss in more detail the components that are screened for FIV and the components that are found to be susceptible to FIV based on the screening criteria. Components that are classified as susceptible to FIV require further evaluation.

Flow-induced vibration mechanisms and screening criteria, which are derived from Regulatory Guide 1.20 and Reference 8.2, are summarized in Table 2-3.

Note that screening is not performed for vibration of thin-walled pipe subject to high velocity internal flow. The most limiting piping segments with small wall thickness and high internal flow velocity are evaluated using the method discussed in Section 3.2.7.

Table 2-2 Nuscale Power Module Components Screened for Susceptibility to Flow-Induced Vibration Mechanisms

NPM Region or Category	Component	Section Number
Components exposed to secondary coolant flow	SGS and CNTS steam piping, MSIVs	Section 2.3.1.1
	SG steam plenum Note 1	Section 2.3.1.2
	DHRS steam and condensate piping	Section 2.3.1.3
	Helical SG tubing Note 1	Section 2.3.1.4
	SG tube inlet flow restrictors	Section 2.3.1.5
	SGS pressure relief valve branch, CNTS FW drain valve branch	Section 2.3.1.6
SG tube supports exposed to primary coolant flow	SG tube support bars	Section 2.3.2.1
	Hanging backing strip	Section 2.3.2.2
	SG tube support spacer	Section 2.3.2.3
	Lower SG support	Section 2.3.2.4
Upper riser assembly exposed to primary coolant flow	Upper riser shells and transition shell	Section 2.3.3.1
	Upper riser bellows	Section 2.3.3.2
	Bellows threaded limit rods	Section 2.3.3.3
	Set screw assemblies	Section 2.3.3.4
	In-core instrument guide tubes (ICIGT) and riser level sensor GTs	Section 2.3.3.5
	Control rod drive (CRD) shaft	Section 2.3.3.6
	CRD shaft support	Section 2.3.3.7
	CRD shaft sleeve	Section 2.3.3.8
Lower riser assembly exposed to primary coolant flow	Lower riser section	Section 2.3.4.1
	Control rod assembly guide tube (CRAGT) assembly	Section 2.3.4.2
	CRAGT support plate	Section 2.3.4.3
	ICIGT funnels and lower riser ICIGTs	Section 2.3.4.4
	Upper core plate	Section 2.3.4.5
Core support assembly exposed to primary coolant flow	Core barrel	Section 2.3.5.1
	Upper support block assembly	Section 2.3.5.2
	Core support assembly mounting brackets	Section 2.3.5.3
	Reflector block	Section 2.3.5.4
	Fuel pin interface	Section 2.3.5.5
	Lower core plate	Section 2.3.5.6

Table 2-2 Nuscale Power Module Components Screened for Susceptibility to Flow-Induced Vibration Mechanisms (Continued)

NPM Region or Category	Component	Section Number
Other RVI exposed to primary coolant flow	Reactor Coolant System (RCS) injection RVI	Section 2.3.6.1
	Pressurizer spray RVI	Section 2.3.6.2
	Flow diverter	Section 2.3.6.3
	Thermowells Note 2	Section 2.3.6.4
	Component and instrument ports	Section 2.3.6.5
	ECCS Valves	Section 2.3.6.6
Primary coolant piping	RCS Injection line tee location	Section 2.3.7.1
	CNTS drain valve tee locations	Section 2.3.7.2

Notes: (1) Component is exposed to primary and secondary coolant flow.
(2) Thermowells also evaluated in NPM piping exposed to secondary coolant flow.

Table 2-3 Flow-Induced Vibration Screening Criteria

Phenomenon	Screening Criteria
Fluid elastic instability (FEI)	• array of cylinders (minimum one row) (i.e., geometry) • array pitch/diameter < 2.0; array must sufficiently confine fluid to allow feedback between adjacent cylinders
Vortex shedding (VS)	• bluff body (or edge of a cavity in line with flow; tube bundle geometry (entrance and exit) (i.e., geometry) • subject to cross-flow • absence of downstream structures to disrupt vortices
Turbulent buffeting (TB)	• subject to turbulent flow (i.e., axial, cross-flow or combination) • component interface that is in load path of one or more components subject to turbulent flow
Acoustic resonance (AR)	• suitable geometry to generate an AR, typically a hollow or cavity • single-phase environment within hollow region/cavity
Leakage flow instability (LFI)	Conditions 1 and 2 are met: 1. narrow annular flow path exists (i.e., geometry) 2. flexible structure in annulus, bounded by fixed surface AND either Condition 3 or Condition 4 is satisfied: 3. annular flow velocity greater than the critical flow velocity for LFI (Section 2.3.8) 4. flow conditions to generate sufficient flow velocity and pressure differential through annular flow path
Galloping/flutter	• non-circular cross section (i.e., geometry) • aspect ratio (length/width) in prevailing direction of flow is less than 4.0 (for tall rectangular structure) and less than 2.0 (for low, long rectangular structure)

2.3.1 Components Exposed to Secondary Flow

The components exposed to secondary flow are contained in the SGs, SGS piping, and DHRS. The SGS transfers heat from the reactor coolant to produce superheated steam, while providing a leak-tight pressure boundary between the primary reactor coolant and the secondary-side coolant. Additionally, the SGs remove residual and

decay heat from the RXC in conjunction with the DHRS following DHRS actuation. The screening of the components exposed to secondary side flow for FIV is discussed in the following subsections.

2.3.1.1 SGS and CNTS Steam Piping, Main Steam Isolation Valves

The steam nozzle is located immediately downstream of the steam plenum (Figure 2-2). Steam flow turns ninety degrees as it exits the steam nozzle and flow transitions into the steam piping. Likewise, there are additional 90-degree bends at the T-connection where the steam piping from the two individual steam plenums that comprise a single SG join to form a single steam header (Figure 2-3). There is the potential for vortices to form due to shedding off the leading edges of these transitions. Similar shedding could potentially occur at the sockolet location connecting to the manual drain valves in the steam line piping (Figure 2-5). When shedding frequencies become close or equal to the acoustic frequencies of the downstream piping, valve bodies, or nozzle bodies, AR can occur. Although vortices could form at these locations, they are not susceptible to vortex shedding lock-in phenomena because the features where the vortices could form do not represent bluff bodies exposed to cross flow. Using the screening criteria, no FIV phenomena are credible for these regions.

The main steam isolation bypass valves are open in normal operation. Because they are open in normal operation, the flow-occluded region is eliminated and AR does not occur at the tee locations where the main steam isolation bypass lines connect to the main steam line.

The CNTS main steam branch connection to the DHRS steam piping (Figure 2-4) and MS drain (Figure 2-5) would screen for AR; however, a delta-spoiler type flow disruptor is added to the leading edge at the two branch connections to preclude the coherent shedding of vortices and the possibility of an AR condition between the shedding frequency and acoustic cavity frequency. This configuration is expected to preclude the onset of AR during operation, and is tested to confirm this during initial startup testing.

Figure 2-2 Steam Nozzle and Downstream Steam Piping

{{

}}2(a),(c),ECI

Figure 2-3 Steam Piping Downstream of RPV Nozzles

{{

}}2(a),(c),ECI

Figure 2-4 Containment System Piping Tees to Decay Heat Removal System Steam Piping

{{

}}2(a),(c),ECI

Figure 2-5 Containment System Main Steam Piping Assembly

{{

}}2(a),(c),ECI

2.3.1.2 Steam Generator Steam Plenum

As shown in Figure 3-1, the SG steam plenums are located at the top of the SG tube bundle and directly above the integrated steam plenum (ISP). The plenum tube sheet region provides the termination point for the helical SG tubes and the plenum internal volume channels steam flow from the SG tubes into the steam nozzle located on the outside of the RPV.

The plenum itself is most comparable to a chamber composed of the primary head and SG tube sheet in a conventional recirculating SG, as it is effectively an independent pressure vessel chamber. Although the outside of the plenum is subject to pressurizer coolant flow, based on the size and construction of the plenum, significant turbulent response is not plausible. The steam plenum is a bluff body; however, based on the SG tubes connecting on the downstream side,

VS would be disrupted. Based on lack of potential leakage flow paths and roughly cylindrical geometry, leakage flow and galloping/flutter are excluded. The sole potential FIV phenomenon to which the steam plenums could potentially be subject is internal AR.

2.3.1.3 Decay Heat Removal System Steam and Condensate Piping

During normal operation, the DHRS is not used, and the DHRS actuation valves are closed. During off-normal operations, the SGS may function in conjunction with the DHRS to remove decay heat and bring the RCS to a safe shutdown temperature. Upon DHRS actuation, the SGS receives feedwater from the DHRS condensate lines. Steam generated by the SGs is routed to the CNTS steam lines as during normal operations.

Figure 2-4 and Figure 2-6 illustrate the DHRS steam piping from the tee at the CNTS steam lines to the DHRS actuation valves, that are closed during normal operation. A flow disruptor is added to the leading edge of the entrance to the DHRS steam piping to prevent the coherent shedding of vortices and possible lock-in condition with the acoustic frequency of the DHRS steam piping. This feature is expected to preclude the onset of AR during operation and is tested to confirm this during initial startup testing.

Figure 2-7 shows the DHRS condensate line connected to the steam generator feed water piping at the cross. One end of the DHRS condensate line is connected to the cross and the other end is connected to the DHRS condenser by decay heat removal nozzles. The DHRS steam and condensate lines represent branch lines in which there is normally no flow during operation. Acoustic resonance is possible for these lines. Within the DHRS condenser, AR in the header assemblies is unlikely to be a concern as the transmitted pressure waves lose energy as they pass through the series of tee junctions (at the condenser tube entrances and exits), eliminating the potential for AR. Using the screening criteria, the DHRS steam and condensate piping is not susceptible to the other FIV mechanisms.

Figure 2-6 Decay Heat Removal System Piping

{{

}}2(a),(c),ECI

Figure 2-7 Steam Generator Feedwater and Decay Heat Removal Piping Assembly

{{

}}2(a),(c),ECI

2.3.1.4 Steam Generator Helical Tubing

The helical SG tubes span the distance between the feedwater and steam plenums shown in Figure 2-8. The tube bundle is composed of 21 columns of tubes contained in the annulus between the RPV shell and the upper riser section. Secondary-feed flow enters the tubes at the feed plenums and boils, producing superheated steam internally along the length of the tubes. As such, the random pressure fluctuations associated with boiling inside the tubes provides a

secondary source of turbulent energy to the tubes in addition to the turbulent forces due to reactor coolant (cross) flow outside the tubes.

Like typical U-tube or straight-tube bundles, the potential for fluid elastic instability (FEI) of the tube bundle exists. Vortex shedding is possible in the upper and lower regions of the tube bundle. Vortex shedding from SG tubes has not been demonstrated to occur in tests of closely-packed tube arrays since the presence of tubes directly downstream disrupts coherent vortex formation. Vibration due to incoherent vortices may exist for the interior SG tubes. These vibrations are accounted for in the turbulent buffeting loads. Based on the tube geometry and the lack of leakage flow paths, leakage and galloping/flutter are excluded.

Figure 2-8 Helical Steam Generator Tube Bundle

{{

}}2(a),(c),ECI

2.3.1.5 Steam Generator Tube Inlet Flow Restrictors

Each individual SG tube requires an inlet flow restriction device to generate a sufficient inlet loss to establish stable, secondary side flow. Each flow restrictor assembly connects to the FW plenum tubesheet and extends into the portion of the SG tube inside the FW plenum tubesheet. The flow restrictor design provides for secondary flow from the FW plenum through the center-flow restrictor mandrel with orifice. The metallic expanding collet and the flanged sleeve, that are in

contact with the SG tube inner diameter, prevent flow and provide for a rigid connection between the flow restrictor assembly and the SG tube. The locking tab prevents loosening of the hex nut during operation, to keep the assembly securely in place. A tack weld between the first and second thread of the mandrel prevents disassembly during operation. Figure 2-9 and Figure 2-10 provide a representation of the center-flow restrictor design. The left side of Figure 2-9 shows the assembly, and the right side shows the assembly installed in the FW plenum tubesheet.

Since there is only one flow path in the assembly, leakage flow is not a concern. Vortex shedding, FEI, AR, gallop, and flutter are precluded by the assembly geometry. The assembly is subject to turbulent buffeting due to the secondary side flow through the center-flow mandrel with orifice.

The flow assessment for cavitation at the SG tubes inlet flow restrictor during density wave oscillations (DWO) is evaluated in Section 3.2.9.

Figure 2-9 Center-flow Restrictor Assembly (left); View as installed (right)

{{

}}2(a),(c),ECI

Figure 2-10 Center-flow Restrictor Assembly - Cross Section View

{{

}}2(a),(c),ECI

2.3.1.6 Steam Generator System Pressure Relief Valve and Containment System Feedwater Drain Valve Branch Piping

A pressure relief valve is on each of the two feedwater lines inside containment as shown in Figure 2-7. The drain valves are below the refueling flange outside of containment, as shown in Figure 2-11. There is one drain valve on each of the two FW lines.

The pressure relief valves and drain valves are connected to the main piping with a short branch of small diameter piping. The fluid in these piping regions is single-phase. The valves are normally closed, and the branch piping represents a flow occluded region connected to the main piping. Vortices may be generated as flow passes the discontinuity in the piping created by the branch. If the vortices generate an acoustic wave coincident with a structural mode, AR could occur in the branch piping lines. Using the screening criteria, the SGS pressure relief valve and CNTS FW drain valve branch piping are not susceptible to the other FIV mechanisms.

Figure 2-11 Containment System Feedwater Piping Assembly

{{

}}2(a),(c),ECI

2.3.2 Steam Generator Supports

The SG steam and feedwater plenums are integral parts of the RPV. The SG helical tubing is provided with supports and lower SG support members, that are welded to the RPV inner wall. In addition to considering these supports in the evaluation of the helical tubing for FIV in Section 2.3.1.4, the supports themselves are assessed to ensure the designs are acceptable to prevent detrimental FIV.

2.3.2.1 Steam Generator Tube Support Bars

Tube supports bars shown in Figure 2-12 span the full height of the helical tube bundle and are anchored at each end by connection to the upper tube support and lower SG support. Based on their geometry, the tube supports are not subject to leakage flow or AR. Based on the confinement of the bars within the tube bundle, where the tortuous flow path creates turbulence, formation of coherent vortices do not occur. The axial alignment of the tube supports provides an aspect ratio greater than 4.0 and an angle of attack of effectively zero thus precluding galloping and flutter.

The SG tube support is further described in FSAR Section 5.4.1, Steam Generators. The modal evaluation for the SG tube support bars is discussed in Section 3.1.

Figure 2-12 Steam Generator Tube Support Assembly (Shown in a Horizontal Installation)

{{

}}2(a),(c),ECI

2.3.2.2 Hanging Backing Strip

Hanging backing strip shown in Figure 2-13 can be considered a “column 0 tube support” and spans the full height of the helical tube bundles. The hanging backing strip is susceptible to turbulent buffeting (TB). Using the screening criteria, the hanging backing strip is not susceptible to the other FIV mechanisms.

Figure 2-13 Hanging Backing Strip

{{

}}2(a),(c),ECI

2.3.2.3 Steam Generator Tube Support Spacer

The SG tube support spacer is installed to react at the base of the column 21 support, as shown in Figure 2-14. {{

}}2(a),(c),ECI Based on their geometry, the SG support spacers are not subject to leakage flow or AR. Vortex shedding from the support is possible. With an aspect ratio of about 2.0 as a low, long rectangle, it is not subject to plunge galloping. The SG support spacer is confined between the tube support bar and RPV inner surface and cannot rotate relative to the tube support. Therefore, torsional galloping is excluded and flutter does not need to be evaluated either.

Figure 2-14 Steam Generator Tube Support and Column 21 Tube Support

{{

}}2(a),(c),ECI

2.3.2.4 Lower SG Supports

Figure 2-15 shows the lower SG supports. The upper SG support bar is welded to the RPV and the ISP and is excluded from analysis due to its rigidity. The lower SG supports are welded to the RPV shell below the SG tube bundle. Individual tube supports are not joined to the lower SG supports. The lower SG supports are designed for lateral support only. Below the tube bundle, VS from the lower SG supports is possible. Based on its form and an aspect ratio of about 3.5 as a low, long rectangle, it is not subject to leakage flow, AR, or plunge galloping. The angle of attack for flow impacting the lower SG supports is likely close to zero; however, flow velocities in this region have not been rigorously developed. Due to the overall support structure stiffness, flutter is most likely excluded; however, analysis is performed to substantiate this conclusion. Torsional gallop should be evaluated.

Figure 2-15 Lower Steam Generator Supports with Inner Steam Generator Columns Removed for Clarity

{{

}}2(a),(c),ECI

2.3.3 Upper Riser Assembly

The upper riser assembly includes the upper riser section and transition section, upper riser bellows, a series of supports for the control rod drive (CRD) shafts, in-core instrument guide tubes (ICIGTs), riser level sensor guide tubes (GTs), and the upper riser hanger assembly. The portions of the upper riser assembly that screen for FIV are identified in the following subsections.

2.3.3.1 Upper Riser Shells and Transition Shell

The two upper riser shells (URSs) and one transition shell, shown in Figure 2-16, are susceptible to parallel flow TB due to upward flow as the fluid enters the riser at the transition, and due to the downward flow on the exterior of the riser. The URSs are not susceptible to FEI, AR, gallop, or flutter due to the geometry. The URSs direct the fluid flow and do not experience cross flow, precluding them from a VS susceptibility.

The upper riser shell is supported by the upper riser hanger in the vertical direction. Horizontally, it is primarily supported by the SG tube supports in the radial direction. The upper riser section itself is an open cylinder. Fluid enters the upper riser section at the transition and turns 180 degrees over the upper edge of the riser.

Flow in the region above the riser is fully turbulent. This region does not represent a cavity, where AR could develop, because it contains the CRD shaft sleeves, ICIGTs, riser level GTs, hot leg thermowells, as well as the SG tubes. Therefore, FIV due to mechanisms other than TB are not credible for the upper riser section.

There are {{ }}$^{2(a),(c),ECI}$ approximately rectangular slots with slot height of {{ }}$^{2(a),(c),ECI}$ on the URS to provide a flow path for boron redistribution. The slots are in four groups, spaced 90 degrees apart on the URS. The slots allow for bypass flow between the riser and the steam generator regions. Note that the height of the slots and inclination angle of {{ }}$^{2(a),(c),ECI}$ degrees are chosen to direct the jet flow downward to decrease the lateral deflection of the reactor coolant flow around the steam generator tubes and to prevent fluid structure interaction between the tubes and the jet. The URS flow slots are similar to other NPM features designed to provide flow, such as the pressurizer baffle plate flow holes and the CRAGT assembly flow holes. The upper riser section flow slots are not susceptible to FIV other than due to turbulent flow.

Figure 2-16 Upper Riser Assembly

{{

}}2(a),(c),ECI

2.3.3.2 Upper Riser Bellows

The upper riser bellows design has two sections of convolutions separated by a shell section as shown in Figure 2-16. On the top side, the bellows shell is welded to the upper riser section, and on the bottom side, the bellows shell is welded to the upper riser transition. The main function of the upper riser bellows is to accommodate differential thermal expansion of the reactor vessel internals, relative to the reactor pressure vessel. The upper riser bellows provide a compressive force in the cold assembled condition of the NPM to ensure the tight fitting at the interface of the upper riser and the lower riser, excluding leakage flow at the interface. The bellows are susceptible to parallel flow TB due to the upward flow as the fluid enters the riser at the transition, and due to the downward flow on the exterior of the riser. In addition, bellows are susceptible to vortex shedding from convolutions. Upper riser bellows are not susceptible to FEI, gallop, or flutter due to the geometry.

2.3.3.3 Bellows Threaded Limit Rods

Threaded limit rods are positioned on the inside of the bellows shell, shown in Figure 2-16, to prevent excessive axial extension of the convolutions during disassembly of the upper NPM. Turbulent buffeting is possible on the threaded limit rods as the fluid moves upward parallel to the component. The rods are not susceptible to FEI, AR, gallop, or flutter due to the geometry. The rods are not subject to cross flow. The tabs to support the limit rods at the top and bottom ends protrude into the flow path and are subject to cross flow. However, the vortices generated would be disrupted by downstream structures, including bellow convolutions and CRD shaft. In addition, the tabs are welded to the bellow shells and are not able to vibrate significantly in lateral direction. Therefore, the component is not susceptible to VS.

2.3.3.4 Set Screw Assemblies

The {{ }}$^{2(a),(c),ECI}$ set screw assemblies, as shown in Figure 2-16, are installed on the upper riser shells to close the clearance between the upper riser and hanging back strips after the riser is inserted. The screws are tightened to close radial gaps in tube support stacks. Figure 2-17 shows the adjustable riser-to-SG interface. The set screw assemblies are susceptible to the turbulent flow inside the riser. They also protrude into the annular flow stream between the upper riser and RPV. Since the screw assemblies protrude into the flow path of the coolant flow, they are also susceptible to the VS. However, since the unsupported length of the set screw assemblies is short, the set screw assemblies are stiff. The natural frequency of the set screw assemblies are expected to be high and the vortex shedding lock-in is not expected to occur. The screw assemblies are not susceptible to FEI, AR, gallop, or flutter due to the geometry.

Figure 2-17 Adjustable riser to SG Interface

{{

}}2(a),(c),ECI

2.3.3.5 In-core Instrument Guide Tubes and Riser Level Sensor Guide Tubes

The ICIGTs and riser level sensor GTs extend from the upper RPV head to the bottom CRD shaft support. On the interior of the ICIGTs reside the in-core instruments that are routed through the pressure boundary at the RPV head and down into the core. On the interior of the riser level sensor GTs reside the level

sensors to measure the water level in pressurizer and upper riser. The ICIGTs interface with the upper RPV head, pressurizer baffle plate and upper riser hanger plate, and four CRD shaft supports. The riser level sensor GTs interface with the upper RPV head, pressurizer baffle plate, upper riser hanger plate, and five CRD shaft supports.

Vortex shedding and turbulent buffeting are possible on the outside of the ICIGTs and riser level sensor GTs as the fluid first moves vertically parallel to the component routing and then turns in the upper plenum to move outward toward the steam plenums.

The clearance between the ICIGT or riser level sensor guide tubes and the CRD shaft support is negligible compared to the riser flow area. Additionally, due to the low pressure differential across the supports, it is not credible that significant flow through this annulus develops to create leakage flow instability of the ICIGT or riser level sensor GTs.

The riser level sensor is a thermal dispersion switch assembly with switches at various levels. The riser level sensor GTs are perforated to allow water flow into and out of the GTs. Vortex shedding and TB could occur at the edges of the perforations; however, the vortices generated are expected to be disrupted by the downstream structure. Using the screening criteria, the geometry of the ICIGTs and riser level sensor GTs precludes FEI, AR, gallop, or flutter.

2.3.3.6 Control Rod Drive Shaft

As shown in Figure 2-18, each CRD shaft passes through the CRD shaft supports as they are routed to the fuel assemblies. The CRD shaft support openings are one of the CRD shaft alignment features and the clearance between the two components is small. Additionally, the flow through the annular flow regions between the CRD shaft and the pressurizer baffle plate is expected to be low. Therefore, leakage flow instability is not credible. The CRD shaft is protected from cross flow and vortex shedding by the CRD shaft sleeves. The CRD shaft is susceptible to TB by the axial turbulent flow in the riser. Using the screening criteria, the CRD shaft is not susceptible to the other FIV mechanisms.

2.3.3.7 Control Rod Drive Shaft Support

The five CRD shaft supports, including one top CRD shaft support, one lower CRD shaft support, and three intermediate CRD shaft supports, are attached to the URS, as shown in Figure 2-18. {{

}}2(a),(c),ECI The ICIGTs and riser level sensor GTs float inside these guide tube riser sleeves. The CRD shaft supports are show in Figure 2-19 and the guide tube riser sleeves are shown in Figure 2-20.

As the primary fluid moves around the support beams, VS and TB may occur. Using the screening criteria, the CRD shaft supports are not susceptible to the other FIV mechanisms.

Figure 2-18 Control Rod Drive Shaft and Guide Tubes with Supports

{{

}}2(a),(c),ECI

Figure 2-19 Control Rod Drive Shaft Supports; Top (Left), Intermediate (Middle), Lower (Right)

{{

}}2(a),(c),ECI

Figure 2-20 Guide Tube Riser Sleeves (shown in red)

{{

}}2(a),(c),ECI

2.3.3.8 CRD Shaft Sleeve

As shown in Figure 2-21, the CRD shaft sleeves extend from the upper riser hanger plate to the top CRD shaft support in the riser. The sleeves shield the CRD shafts from cross flow in the upper riser. Some of the sleeves have the additional function of bearing the load of the riser. The load bearing sleeves have a thicker diameter than the non-load bearing sleeves. The load bearing sleeves are threaded into the hanger plate and top CRD shaft support. The non-load bearing

sleeves are threaded into the hanger plate and are welded at the CRD shaft support.

The sleeves represent a cylinder in cross flow and are susceptible to VS. During steady state operation, there is negligible pressure difference between the riser outlet and the pressurizer. Due to the momentum of the flow as it exits the riser, it is possible that some flow passes through the annular flow regions between the CRD shaft and the sleeve. This flow is expected to be low, based on the low driving force. Therefore, leakage flow instability is not credible. The CRD shaft sleeves are susceptible to TB and VS. Using the screening criteria, the CRD shaft sleeves are not susceptible to the other FIV mechanisms.

Figure 2-21 Upper Riser Hanger Assembly

{{

}}2(a),(c),ECI

2.3.4 Lower Riser Assembly

The lower riser assembly includes the lower riser section, CRA guide tubes, CRA guide tube support plate, the in-core instrument guide tube funnels welded to the CRA guide tube support plate, and the upper core plate. The portions of the lower riser assembly that screen for FIV are identified in the following subsections.

2.3.4.1 Lower Riser Section

The lower riser section is the cylindrical section in the lower riser assembly, as shown in Figure 2-22. This section transfers the loads from the upper riser, lower riser interface, and control rod assembly guide tube (CRAGT) support plate to the upper core plate. It also separates the up-flowing primary coolant above the core from the down-flowing primary coolant in the downcomer. The lower riser section is susceptible to TB due to parallel flow and vortices generated by the feed plenums. The open cylindrical shape precludes the lower riser section from being susceptible to FEI, AR, leakage flow, gallop, or flutter. The lower riser section is not susceptible to VS because no part of the component is opposing the flow path.

There are four {{ }}$^{2(a),(c),ECI}$ holes on the lower riser assembly to provide a flow path for boron redistribution. The holes are uniformly spaced, with two of them in line with the reactor recirculation valve (RRV) penetrations on the upper RPV. Using the screening criteria, the lower riser section holes are not susceptible to FIV mechanisms other than due to turbulent flow.

Figure 2-22 Lower Riser Assembly

{{

}}2(a),(c),ECI

2.3.4.2 Control Rod Assembly Guide Tube Assembly

The CRAGT supports the CRAs at varying amounts of control rod insertion, as shown in Figure 2-23. The CRAGT assembly includes CRA cards, the CRA lower flange, the CRA guide tube, and the CRA alignment cone. The CRA cards, lower flange, and alignment cone are welded to the CRAGT guide tube to form the CRAGT assembly. The CRAGT assemblies are supported by the upper core plate and the guide tube support plate (Section 2.3.4.3).

The CRAGT components have many sharp edges to cause VS and TB. However, the vortices generated are disrupted by the downstream structure. The CRAGT assembly is not susceptible to leakage flow because there is not an annular flow path with a flexible boundary. Using the screening criteria, the CRAGT is not susceptible to FIV mechanisms, other than TB.

Figure 2-23 Control Rod Assembly Guide Tube Assembly

{{

}}2(a),(c),ECI

2.3.4.3 Control Rod Assembly Guide Tube Support Plate

The CRAGT support plates are above the CRAGT assembly, as depicted in Figure 2-22. Similar to the CRAGT assembly, the support plate is subject to turbulent flow. The ligaments connecting the guide tube holes represents a bluff body subject to cross flow. Therefore, TB and VS are applicable mechanisms. Using the screening criteria, the CRAGT support plate is not susceptible to the other FIV mechanisms.

2.3.4.4 In-core Instrument Guide Tube Funnels and Lower Riser In-core Instrument Guide Tubes

The ICIGT funnels and lower riser ICIGTs, as shown in Figure 2-22, are to help align the in-core instrument during reinsertion. The lip of the funnel is welded to the CRAGT support plate and the end of the funnel is welded to the lower riser ICIGTs, which extend to and float in the upper core plate flow holes. The funnels and ICIGTs are susceptible to TB on the outside surface as the fluid moves vertically parallel to the component. The clearance between the ICIGTs and the upper core plate flow holes is negligible compared to the riser flow area. Additionally, due to the low pressure differential across the upper core plate, it is not credible that significant flow through this annulus develops to create leakage flow instability of the ICIGT. Using the screening criteria, the funnels and lower riser ICIGTs are not susceptible to the other FIV mechanisms.

2.3.4.5 Upper Core Plate

The upper core plate is located below the CRAGT assemblies, as shown in Figure 2-22. The upper core plate is subject to turbulent flow and the ligaments connecting the holes represents a bluff body subject to cross flow. Therefore, TB and VS are applicable mechanisms. The upper core plate is thicker and stiffer than the CRAGT support plate so the response of the upper core plate to these mechanisms is expected to be bounded. Using the screening criteria, the upper core plate is not susceptible to the other FIV mechanisms.

2.3.5 Core Support Assembly

The core support assembly is located in the bottom region of the RPV, below the RPV flange. The core support assembly includes the core barrel, reflector block, upper support blocks, bolt and alignment pin, lower core plate, fuel pin interface, and core support assembly mounting brackets. While many of the components are exposed to turbulent flow and some are exposed to cross flow, vibration of these components or components in the load path are not expected based on the component weights and stiffness. The portions of the core support assembly that screen for FIV are identified in the following subsections.

Figure 2-24 Core Support Assembly

{{

}}2(a),(c),ECI

2.3.5.1 Core Barrel

The core barrel is a cylinder designed to carry the core support loads and separate the fluid in the downcomer from the fuel, as denoted in Figure 2-24. The core barrel is susceptible to TB. Using the screening criteria, the core barrel is not susceptible to the other FIV mechanisms.

2.3.5.2 Upper Support Block

The upper support block is attached to the core barrel and opposes the fluid as it travels through the downcomer, as shown in Figure 2-24. The upper support block is susceptible to VS and TB phenomena. Using the screening criteria, the upper support block is not susceptible to the other FIV mechanisms.

2.3.5.3 Core Support Assembly Mounting Brackets

The core support assembly mounting brackets, as shown in Figure 2-25, transfer the dead weight, seismic, and accident loads from the lower core plate to the lower head of the RPV. The core support assembly mounting brackets oppose the fluid flowing through the downcomer into the lower plenum and are susceptible to TB phenomena. Since vortices generated when the flow passes the mounting brackets are expected to be disrupted at the RPV bottom, the core support assembly mounting brackets are not susceptible to VS. Using the screening criteria, the mounting brackets are not susceptible to the other FIV mechanisms.

Figure 2-25 Core Support Assembly Mounting Brackets and Flow Diverter

{{

}}2(a),(c),ECI

2.3.5.4 Reflector Block

The reflector blocks are aligned by pins and stacked on the lower core plate inside the core barrel, as denoted in Figure 2-24. Primary coolant flows through small channels in the reflector and the inner surface of the reflector is subject to turbulent core flow. The only mechanism applicable to the reflector block is TB. Using the screening criteria, the reflector block is not susceptible to the other FIV mechanisms.

2.3.5.5 Fuel Pin Interface

The fuel top and bottom nozzles interface with fuel pins that are installed in the upper and lower core plates, as shown in Figure 2-26. This interface is a location for mechanical wear primarily driven by the cross flow within the core and is susceptible to TB. Using the screening criteria, the fuel nozzle to the fuel pin is not susceptible to the other FIV mechanisms.

Figure 2-26 Typical Fuel Nozzle-to-Fuel Pin Interface at Lower Core Plate

{{

}}2(a),(c),ECI

2.3.5.6 Lower Core Plate

The lower core plate is located below the fuel assemblies, as depicted in Figure 2-24. The lower core plate is subject to turbulent flow and also represents a bluff body subject to cross flow. There is no cavity region downstream of the lower core plate where AR could form. The structures downstream of the lower core plate are primarily narrow flow channels composed of fuel assemblies. Therefore, TB and VS are applicable mechanisms. Using the screening criteria, the lower core plate is not susceptible to the other FIV mechanisms including AR, which cannot form in the highly turbulent conditions downstream of the lower core plate.

2.3.6 Other Reactor Vessel Internals

There are other design features located in the primary and secondary coolant flow paths that require FIV screening. These consist of instrumentation and system connections that support interfacing systems. For the NPM design, the majority of the RPV connections are located in the steam space of the pressurizer. This region is always steam and is not exposed to high average flow rates, even under transient and accident conditions, due to the large cross sectional area of the region. Therefore, for the majority of the instrument and interfacing system connections in the NPM design, degradation due to FIV is not credible. The portions of the other reactor vessel internals that screen for FIV are identified in the following subsections.

2.3.6.1 Reactor Coolant System Injection Reactor Vessel Internal

The Reactor Coolant System (RCS) injection feeds into the injection RVI, which injects primary coolant into the upper riser and connects to the RCS injection piping through a port in the RPV wall. The RCS injection line is routed from a flange in the RPV wall through the URS into the up-flowing region of the upper riser, as shown in Figure 2-27. The line is susceptible to VS and TB. Using the screening criteria, the RCS injection RVI is not susceptible to the other FIV mechanisms.

Figure 2-27 Reactor Coolant System Injection Reactor Vessel Internals

{{

}}2(a),(c),ECI

2.3.6.2 Pressurizer Spray Reactor Vessel Internal

The pressurizer spray lines and nozzles are attached to the upper RPV head and extend downward into the steam region of the pressurizer. Fluid is pumped through these components to provide the pressurizer spray. The pressurizer spray reactor vessel internals are susceptible to TB as there is a large pressure loss across the nozzle and flow rates through the spray line piping are turbulent when spray flow is used. Using the screening criteria, the pressurizer spray lines and nozzles are not susceptible to the other FIV mechanisms.

2.3.6.3 Flow Diverter

A flow diverter is located on the RPV bottom head under the core support assembly, as shown in Figure 2-25. This flow diverter smooths the turning of the reactor coolant flow from the downward flow outside the core barrel to upward

flow through the fuel assemblies. The flow diverter reduces flow turbulence and recirculation, and minimizes flow-related pressure loss in this region. Because flow in this region is turbulent, the flow diverter is susceptible to TB. Using the screening criteria, the flow diverter is not susceptible to the other FIV mechanisms.

2.3.6.4 Thermowells

Within the primary coolant flow path, RCS temperature instruments are installed in thermowells located at the entrance to the SG tubes and in the downcomer. Thermowells are welded to the RPV. Thermowells are also used for instrumentation and used to measure temperature in secondary side piping. In locations where they are used, thermowells extend into the flow path and are exposed to turbulent cross-flow conditions. Therefore, they are susceptible to VS and TB. Using the screening criteria, the thermowells are not susceptible to the other FIV mechanisms.

2.3.6.5 Component and Instrument Ports

Acoustic resonances due to the generation of vortices that form acoustic waves at closed branch lines are evaluated. Penetrations that create a hollow cavity and that are located in regions with adjacent flow are susceptible to AR. Due to the integral design of the NPM, the RPV contains a few penetrations along the primary coolant flow path. For the NPM design, the only components that meet this criterion are the primary coolant flow sensors and RRVs, which are both located in the downcomer. Due to the flow conditions and geometry in these regions, no FIV mechanisms other than AR are credible for component and instrument ports.

2.3.6.6 ECCS Valves

During an accident the emergency core cooling system (ECCS) may be actuated, allowing flow through the ECCS valves. There are flow limiting venturis included in the ECCS valves to limit flow out of the RPV during postulated inadvertent opening events in safety analyses. The ECCS valves are an angle globe valve design, wherein flow makes a 90-degree turn and passes around the valve disc when the valve is open. Flow through both the RRV and the RVV is shown in Figure 2-28 (note the venturi feature is not shown). For the RRV, flow can go in either direction. The valve disc is not in direct cross flow and downstream structures (the valve 90-degree turn) are present to disrupt potential vortices generated by the valve internals. The valve body is designed for reaction loads of valve discharge and seismic loads, which are significantly more severe than TB loads on the valve. Therefore, ECCS valves screen out for TB although it is subject to the load. Due to the geometry in the ECCS valves, no FIV phenomena are credible for through-valve flow.

Figure 2-28 Emergency Core Cooling System Valve Internal Flow Diagram

{{

}}2(a),(c),ECI

2.3.7 Primary Coolant Piping

Piping that is a part of the NPM is screened for susceptibility to FIV. Two piping regions that are not judged to be susceptible to FIV mechanisms are the piping for the control rod drive system cooling water, and the piping that supports containment flooding, draining, and evacuation.

Consistent with other NPM piping, AR is the mechanism potentially applicable for these regions. These piping segments contain tees that connect from the main piping run to drain valves; however, those piping segments do not contain primary coolant or transport fluid at high velocities; therefore, they are not included in the FIV screening. Other regions of this piping do not contain flow occluded regions and are therefore not susceptible to acoustic resonance.

2.3.7.1 Reactor Coolant System Injection Line Tee Location

Inside containment, the upper region of the RCS injection line contains one tee location that connects to the emergency core cooling system trip/reset valves. During normal operation, there is no flow in the valve reset lines. One tee connection is provided in the upper region of the injection line. Vortices could form at the tee location and the small diameter lines leading to the trip/reset valves represents a flow occluded region. Therefore, the tee location is susceptible to AR. Using the screening criteria, no other FIV mechanisms are credible for this location.

2.3.7.2 Containment System Drain Valve Tee Locations

The CNTS provides drain locations between the CNTS isolation valves and the NPM disconnect flanges that are connected to the main piping run using a tee in

the following CNTS piping segments: RCS injection, CVC pressurizer spray, CVC discharge, and RPV high point degasification. Vortices could form at the tee locations and the piping leading to the normally shut drain valves represent a flow occluded region. Therefore, these tee locations are susceptible to AR. Using the screening criteria, the CNTS drain valve tee locations are not susceptible to the other FIV mechanisms.

2.3.8 Leakage Flow Instability Screening Using Critical Gap Velocity

Reference 8.14 and Reference 8.15 define a methodology for evaluating the hydrodynamic added mass, damping, and stiffness due to the fluid-structure interaction associated with leakage flow to determine the onset of instability. Added damping consists of the positive damping due to the squeeze film effect and the damping induced by the change in the fluid velocity within the gap, which could be negative owing to the delay caused by the fluid inertia. When the total damping (i.e., sum of the structural damping and added damping due to fluid-structure interaction) is negative, the energy input to the structure by the fluid exceeds the energy dissipated and the onset of instability occurs.

The methodology of Reference 8.14 and Reference 8.15 applies to a one-dimensional axial flow in the short tapered annular passage as shown in Figure 2-29 with two conditions to be satisfied:

1. Small gap assumption $H_o / L \ll 1$
2. Short gap assumption $\frac{2L}{\pi D} \ll 1$

Where H_o is the gap, L is the passage length, and D is the shaft diameter as shown in Figure 2-29.

For the NPM-20 components evaluated for the LFI, which are listed in Table 2-4, the small gap assumption is satisfied, but the short gap assumption is not satisfied. However, per Reference 8.23, which studied the LFI in an annulus, the added fluid damping increases as the length of the annulus increases. Therefore, it is appropriate to use the methodology of Reference 8.14 and Reference 8.15 for the evaluation of NPM-20 components susceptibility to LFI. Note that theoretical values obtained using the methodology correspond well to those obtained from experiments (Reference 8.16)

Figure 2-29 Geometry of Annular Leakage Path for LFI Evaluation

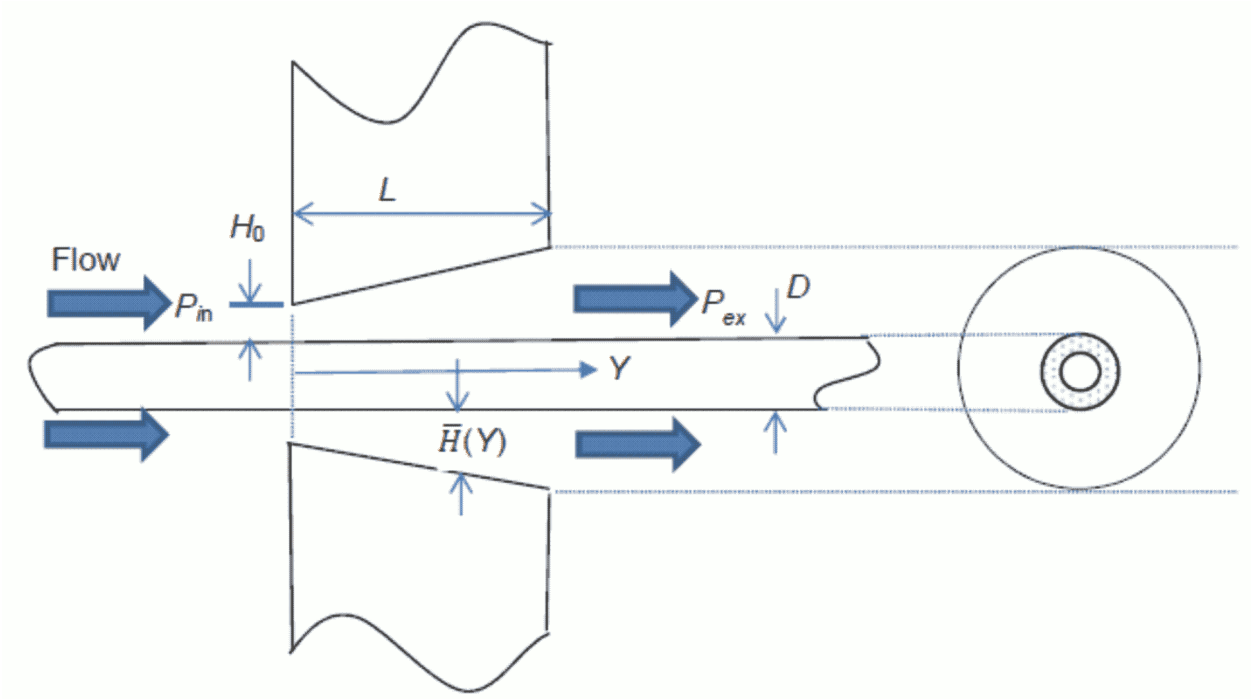

The method in Reference 8.14 and Reference 8.15 is used to determine the critical gap velocity, at which the hydrodynamic damping becomes negative. The critical gap velocity is compared to the steady-state inlet gap velocity calculated using a formula from Reference 8.17 to determine whether the components are susceptible to the LFI. Note that the critical gap velocity thus determined conservatively assumes zero structural damping. The flow velocity at which the total damping becomes negative and the LFI onset occurs is higher than the critical gap velocity based only on the hydrodynamic damping.

The results in Table 2-4 show that the inlet gap velocity is lower than critical gap velocity with large margin. The pressure drop across the channels is also low. In addition, for all locations, the total stiffness is positive for the velocities up to the critical velocity, indicating that static instability due to negative stiffness does not occur. Therefore, the quantitative evaluations indicate that LFI is not a concern for leakage paths at the CRD shaft, ICIGT/riser level sensor GT, and lower riser ICIGT. No additional testing or analyses are recommended for these components.

Table 2-4 Reactor Vessel Internals Components Screened for Leakage Flow Instability

RVI Components		Pressure Drop (psi)	Flow Direction	Inlet Gap Velocity (in/sec)	Critical Gap Velocity (in/sec)
Interior	**Exterior**				
CRD shaft	Pressurizer baffle plate and CRD shaft sleeve	{{			
CRD shaft	CRD shaft sleeve				
CRD shaft	Middle/lower CRD shaft support [1]				
CRD shaft	CRD shaft alignment cone				
ICIGT/Riser level sensor GT	Top/middle CRD shaft support				
ICIGT/Riser level sensor GT	Lower CRD shaft support				
Lower riser ICIGT	Upper core plate				}}2(a),(c),ECI

Notes: (1) The LFI evaluation for the middle CRD shaft support bounds the lower CRD shaft support since the pressure drop over middle CRD shaft support is higher and modal frequency is lower.

(2) The steady state gap velocity is conservatively calculated using the pressure drop of {{ }}2(a),(c),ECI psi over the top and middle CRD shaft support.

2.4 Regulatory Requirements

Consistent with Regulatory Guide 1.20, Revision 4, Section C.2, the prototype CVAP for the NPM is composed of three sub-programs. The program includes

- a vibration and stress analysis program.
- a vibration and stress measurement program.
- an inspection program.

The analysis program uses theoretical analysis to predict the natural frequencies, mode shapes, and structural responses of the NPM components to sources of flow excitations.

The measurement program consists of prototype testing that is used to validate the analysis program inputs, results, and margins of safety. Prototype testing consists of separate effects and initial startup tests. The measurement program verifies the structural integrity of the NPM components. If discrepancies are identified between the analysis and the measurement programs, reconciliation is performed.

The inspection program consists of inspections of the applicable NPM components before and after initial startup testing in order to confirm that the vibratory behavior of the susceptible components is acceptable.

To finalize the CVAP, two additional technical reports are developed. The first report (Reference 8.13) contains details on the measurement program and inspection requirements. Upon completion of validation testing and inspection, the second report provides the post-test evaluation and inspection program results. In this second report, the differences between the expected and measured experimental results are either resolved or confirmed to be in the analytically predicted allowable ranges.

2.5 Classification of NuScale Power Module

Regulatory Guide 1.20 provides guidance to verify the structural integrity of the NPM internals susceptible to FIV. The verification measures depend upon the classification of the internals.

The NPM represents a unique design in its size, arrangement, and operating conditions, although its technology is based on proven light water reactor designs with long operational experience. Accordingly, the first operational NPM is classified as a prototype in accordance with RG 1.20. After the first NPM is qualified as a valid prototype, subsequent NPMs are classified as non-prototype.

3.0 Vibration Analysis Program

The analysis program begins with a list of FIV phenomena and a list of components that could be subjected to these phenomena. Screening criteria for each FIV phenomena are developed from literature, as discussed in Section 2.3.

Due to the very low primary coolant flow rates and passive safety designs, many regions of the NPM are not susceptible to FIV and do not meet FIV screening criteria. For example, the annular region between the outside of the RPV and the inside of the CNV is similar in geometry to the core barrel and reactor vessel of conventional PWRs, which is a location typically susceptible to FIV. For the NPM design, this region only contains liquid when the NPM is filled with reactor pool water in preparation for refueling, and during accident scenarios when primary or secondary coolant condenses on the CNV wall and accumulates in the annular space. In both scenarios, the bulk flow rates in the annular region are laminar and eventually settle into static, pool conditions. Therefore, while this region appears similar to a region that would typically screen for FIV in conventional reactor designs, FIV is not a concern in this region for the NPM design.

For NPM components that meet the screening criteria for FIV mechanisms, additional analysis is performed to confirm whether the structure or component is susceptible to the FIV phenomena. For the NPM components that are evaluated for TB, the response of these structures, in terms of vibrational amplitude and stress, to this source of flow excitation is determined.The FIV phenomena evaluated for NPM components are:

- fluid elastic instability (Section 3.2.1)
- vortex shedding (Section 3.2.2)
- turbulent buffeting (Section 3.2.3)
- acoustic resonance (Section 3.2.4)
- leakage flow instability (Section 3.2.5)
- flutter and gallop (F/G) (Section 3.2.6)
- piping subject to high velocity internal flow (Section 3.2.7)

The analysis program provides methodologies to analyze the screened components for each type of FIV mechanism. This analysis work is divided into two categories:

- developing FIV inputs that are common to each of the analyses or components described in Section 3.1
- developing specific analyses to determine the susceptibility and response of the components to sources of flow excitation, described in Section 3.2

For all phenomena with the exception of TB, the FIV mechanisms are characteristic of a strong fluid-structure coupling system. The NPM components are designed so there is a sufficient margin of safety to the potential onset of these FIV phenomena. Turbulent buffeting occurs when a component is subject to turbulent flow, which is the dominant flow condition of the primary and secondary coolant. For TB, the fluid-structure coupling is

weak and results in low amplitudes of vibration. Provided the impact stresses and fatigue usage are not detrimental to the component or structure over the design life, the acceptance criteria for this source of flow excitation are met.

Although exclusion of many FIV phenomena for a particular component may appear obvious based on inspection, use of the screening criteria enforces rigor and ensures that the basis for determining the required analysis is transparent. The FIV analysis results demonstrate that many components have large margins of safety. The margin of safety is the means by which structural integrity against FIV degradation is assured.

The applicability of the FIV phenomena to components in the NPM is summarized in Table 3-1 and the components are identified in Figure 3-1. The locations of the components are discussed in detail in Section 2.3. The following subsections provide an overview of the analysis program.

The scope of the measurement program is determined based on the results of the analysis program. Components included in the measurement program are discussed in Reference 8.13.

Table 3-1 Nuscale Power Module Components and Their Susceptibility to Flow-Induced Vibration Mechanisms

NPM Component Category	Component	Flow-Induced Vibration Mechanism [3]					
		FEI	VS	TB	AR	LFI	F/G
Components exposed to secondary side flow	SG steam plenum [Note 1]	-	-	-	▲	-	-
	DHRS condensate piping	-	-	-	▲	-	-
	Helical SG tubing [Note 1]	▲	▲	▲	-	-	-
	SG tube inlet flow restrictors	-	-	▲	-	-	-
	SGS pressure relief valve and CNTS FW drain valve branch piping	-	-	-	▲	-	-
SG tube supports	SG tube support bars	-	-	▲	-	-	-
	Hanging backing strip	-	-	▲	-	-	-
	SG tube support spacer	-	▲	▲	-	-	-
	Lower SG support	-	▲	▲	-	-	▲
Upper riser assembly	Upper riser shells and transition shell	-	-	▲	-	-	-
	Upper riser bellows	-	▲	▲	-	-	-
	Bellows threaded limit rods	-	-	▲	-	-	-
	Set screw assemblies	-	-	▲	-	-	-
	ICIGTs and riser level sensor GTs	-	▲	▲	-	-	-
	CRD shaft	-	-	▲	-	-	-
	CRD shaft support	-	▲	▲	-	-	-
	CRD shaft sleeve	-	▲	▲	-	-	-

Table 3-1 Nuscale Power Module Components and Their Susceptibility to Flow-Induced Vibration Mechanisms (Continued)

NPM Component Category	Component	Flow-Induced Vibration Mechanism [3]					
		FEI	VS	TB	AR	LFI	F/G
Lower riser assembly	Lower riser section	-	-	▲	-	-	-
	CRAGT assembly	-	-	▲	-	-	-
	CRAGT support plate	-	▲	▲	-	-	-
	ICIGT funnels and lower riser ICIGTs	-	-	▲	-	-	-
	Upper core plate	-	▲	▲	-	-	-
Core support assembly	Core barrel	-	-	▲	-	-	-
	Upper support block	-	▲	▲	-	-	-
	Core support assembly mounting brackets	-	-	▲	-	-	-
	Reflector block	-	-	▲	-	-	-
	Fuel pin interface	-	-	▲	-	-	-
	Lower core plate	-	▲	▲	-	-	-
Other RVI	RCS injection RVI	-	▲	▲	-	-	-
	Pressurizer spray RVI	-	-	▲	-	-	-
	Flow diverter	-	-	▲	-	-	-
	Thermowells Note 2	-	▲	▲	-	-	-
	RRV and instrument ports	-	-	-	▲	-	-
Primary coolant piping	Piping tees with no branch flow	-	-	-	▲	-	-

Notes: (1) Component is exposed to primary and secondary coolant flow.

(2) Thermowells also evaluated in NPM piping exposed to secondary coolant flow.

(3) The triangle symbol indicates a component meets the screening criteria for the FIV mechanism and requires evaluation in the analysis program. Dashes indicate the mechanism is not credible for the component.

Figure 3-1 Nuscale Power Module Components Susceptible to Flow-induced Vibration

{{

}}2(a),(c),ECI

3.1 Analysis Program Inputs

For components that screen for FIV, analysis is performed to determine component susceptibility. The general criterion used to determine if testing is required to verify an analytical input, method, or result is the calculated margin of safety.

The margin of safety is the means by which structural integrity against FIV degradation is assured. For strongly-coupled FIV mechanisms, the percentage difference between the analytically predicted value and the acceptance criteria that represents the predicted onset of the mechanism for a component is the margin of safety. For TB, safety margins are evaluated for the analytically predicted fatigue against the limits that are acceptable over the component design life.

The safety margin for most mechanisms and components is greater than 100 percent. To ensure that testing is performed to validate a sufficient breadth of the analysis program, a safety margin of 100 percent is specified as the limit below which analytical inputs, methods, and safety margins are validated.

The following sections discuss the analysis program inputs, many of which are common among the different FIV analyses, as identified in Table 3-2. These inputs include structural natural frequencies and mode shapes, system hydraulic models (flow velocities), and component damping. Analysis program methods and results are provided in Section 3.2.

Table 3-2 Selected Common Inputs for Flow-induced Vibration Analysis

Phenomena	Structural Natural Frequency (f_n) Section 3.1.1	Structural Mode Shape (φ) Section 3.1.1	Flow Velocity (U) Section 3.1.2	Damping Ratio (ζ) Section 3.1.3
FEI	▲	▲	▲	▲
VS	▲	▲ [1]	▲	▲ [1]
TB	▲	▲	▲	▲
AR	-	-	▲	-
LFI	▲	▲	▲	▲
F/G	▲	-	▲	-

Note 1: Mode shape and damping are used in the SG tube and ICIGT vortex shedding analysis. These inputs are not required for vortex shedding analysis of other susceptible components.

3.1.1 Structural Natural Frequency and Mode Shapes

The natural frequencies and mode shapes of the structures are required for FEI, VS, TB, LFI, and F/G analyses. Using the finite element analysis (FEA) software ANSYS (Reference 8.10), relatively complex shapes, such as a helical SG tube with transition bends, can be modeled. Once appropriate finite element models are created, developing physically accurate boundary conditions, such as the interface between the tubes and tube supports or the hydrodynamic interaction between a structure and

the surrounding fluid, require sensitivity studies and potentially confirmatory testing. Based on these considerations, two analytical focus areas in the FIV structural model development are the definition of boundary conditions and modeling of hydrodynamic mass effects.

Based on these considerations, three analytical focus areas are indicated for the FIV structural model development. These include:

- definition of boundary conditions
- modeling of hydrodynamic mass effects
- verification of frequency and mode shape results

Boundary conditions for geometries where small gaps may exist, such as between a CRD shaft and its support, may increase uncertainties. These clearances may lead to non-linear behavior and the assumptions used in establishing the boundary conditions at these locations may affect structural frequencies. A CRD shaft support may be “inactive” if a sufficiently large clearance exists between the CRD shaft and the support. At locations where there is the potential for an inactive support condition, the frequency and mode shape evaluation accounts for the limiting expected support arrangement in order to determine bounding structural frequencies and mode shapes. The SG tubes are evaluated with sliding and fixed boundary conditions to represent variability in the contact at the tube supports.

The effect of the surrounding fluid (e.g., hydrodynamic mass) also affects structural frequencies. Typically, simplified “lumped mass” approaches are employed to account for the effect of surrounding fluid on structural frequencies; the mass of the surrounding fluid is included in determining a total mass of the structure for analytical purposes.

In general, analytical models consider the normal design conditions and do not consider all possible uncertainties and biases, such as those associated with manufacturing tolerance and material property allowable ranges. Where possible, values are selected to provide bounding frequency and mode shape results. The selection of mesh size for the structural models are justified through mesh sensitivity studies that indicate that the selected mesh size is appropriate for the frequency range of interest. As part of the pre-verified status of the ANSYS software, software test cases for modal analysis were validated against known solutions for common geometries, using a variety of element types and boundary conditions. The performance of mesh sensitivity studies and test cases ensures that ANSYS is providing reasonable outputs for the given inputs. The methodology for selecting the mesh densities, boundary conditions, and fluid loading for the SG tubes is to be validated against the TF-3 test results. The boundary conditions used in the current design analysis are informed by modal testing at the TF-3 facility to provide the most prototypic results possible at this time. Reference 8.13 provides additional information on the TF-3 test program.

3.1.1.1 Steam Generator Modal Analysis

SG full bundle models and single column tube models are created using ANSYS finite element analysis software capable of performing modal analysis of structures. Modal analysis is performed using the SG full bundle and single tube models to evaluate the frequency response of the SG tubes. A comparison between full bundle and single tube model results validates the use of the single tube models.

The single column ANSYS model for each column contains the two bounding tubes, one at each end of a row of tubes in the tubesheet. SG tubes are modeled with beam elements and tube supports are modeled with shell elements. An effective density for the SG tubes is used which incorporates the nominal Alloy 690 metal mass, the contained secondary fluid mass, and the hydrodynamic mass, which is approximated as the displaced primary fluid mass. Using thermal hydraulic analysis results, the effective density is calculated as a function of elevation due to changing primary and secondary coolant properties as a function of tube length. Figure 3-2 shows the elevation discretization considered for column 11 tubes. SG tube nodalization is chosen to ensure a sufficient number of nodes at the {{ }}$^{2(a),(c),ECI}$. A mesh sensitivity study is performed to validate the tube mesh size used in the single tube model. The geometry for representative tubes in columns 1, 11 and 21 are shown in Figure 3-3.

Figure 3-2 Visualization of the 11 bins along the SG height to account for varying fluid density

{{

}}2(a),(c),ECI

The model uses {{ }}2(a),(c),ECI elements to represent the tube supports.
{{

}}2(a),(c),ECI

In the single tube models, the supports are given a near-zero density. This excludes the tube supports from modal mass participation results, while including the calculated stiffness of the effective tabs. Tube end nodes have all degrees of freedom (DOFs) constrained to simulate the connection where the tubes are inserted and welded to the tubesheets.

Figure 3-3 Representative tubes for single tube models

{{

}}2(a),(c),ECI

The ANSYS model of the full bundle SG is an assembly of all 21 columns of tubes and tube supports, as well as the surrounding structures such as the RPV shell and upper riser. {{

}}2(a),(c),ECI Fluid and material properties are evaluated at normal operating conditions. The geometry for the full bundle model is shown in Figure 3-4, with the details of the column 11 SG tubes and supports shown in Figure 3-5.

Figure 3-4 Full bundle SG model

{{

}}2(a),(c),ECI

Figure 3-5 Model for Column 11 tubes and supports

{{

}}2(a),(c),ECI

{{

}}2(a),(c),ECI

In the ANSYS models, {{

}}2(a),(c),ECI

Figure 3-6 shows a 3D model view of a segment of a SG tube support and compares to the simplified ANSYS model representation.

Figure 3-6 Tube to tube support contacts (column 11 shown)

{{

}}2(a),(c),ECI

The modal analysis for single tube models are performed with modes up to 300 Hz being calculated. Two separate modal analyses are performed to consider tube to tube support connections with a fixed configuration and with a sliding configuration. A bonded contact setting in ANSYS has the contact element nodes fixed onto the target elements. This represents the case where there is sufficient friction between the tube and the support to restrain movement along the tube axis through the tube support. With the no separation contact setting, the contact element nodes can slide on the target element faces. This represents the case where there is zero friction between the tube and the support, allowing the tube to slide through the support bar. These cases bound the realistic situation with certain frictional forces that make the model nonlinear. The top and bottom ends of the tube supports and the nodes of each tube support tab tip-edge have all DOFs constrained since the single tube models are intended to simulate the modal responses of the tubes.

The fixed cases show a reduced mass participation in the horizontal directions when compared to the sliding cases for the same column. In general, restricting sliding of the tube results in a stiffer structure with a corresponding upward shift in frequency.

A finer tube mesh is created for column 11 as a sensitivity study in order to show that the single tube models are sufficiently refined to capture relevant modes below 300 Hz. Both the fixed and sliding boundary conditions are compared in the x, y, and z directions between the refined mesh models and the regular mesh models for a total of 6 comparisons. The cumulative mass participations for the modes demonstrate good agreement between the mesh sizes. The maximum percent difference in modal frequencies between the regular mesh and the refined mesh is {{ }}$^{2(a),(c),ECI}$ for modes up to 300 Hz for both the fixed and sliding cases.

Modal analysis is performed for the full bundle model up to 100 Hz. The full bundle modal results are compared to the single tube results for the fixed configuration case. The comparison table shows that the tube modes match very well between the full bundle and single tube models. Modes for the transition bends and long spans were chosen for comparison in order to cover a variety of mode types. This close matching between models implies that the supporting structures are much stiffer than the tubes, and therefore the supporting structures can be replaced with direct boundary conditions, as used in the single tube models. The mode comparison summary is provided in Table 3-3.

Table 3-3 Mode comparison between full bundle and single tube models

Column	Full Bundle Frequency (Hz)	Single Tube Frequency (Hz)	Mode Type
{{			
			}}2(a),(c),ECI

(1) the lowest beam mode for column 1 is above 100 Hz which has not been extracted in the full bundle model.

3.1.2 Flow Velocity

3.1.2.1 Steady-State Velocity Analysis

Appropriate representation of the flow conditions is essential to performing the analysis of FIV phenomena. The RCS and secondary-flow rates for regions of the NPM are determined and verified using thermal-hydraulic (TH) and computational fluid dynamics (CFD) analyses. Additionally, separate effects tests have been performed to validate the significant inputs in the TH modeling, such as core and SG form losses and SG performance, which is a significant contributor to the natural circulation buoyant force. The TH analysis provides validated maximum design flow rate results based on testing. Maximum design flow rates (or higher) are used in all FIV evaluations. Maximum design flow represents the highest expected primary coolant flow rate used in design and safety analyses and is the licensing basis flow rate; operation above this flow rate is not permitted without evaluation against safety analysis limits.

Several biases are applied in the TH analysis to ensure the calculation of a bounding maximum design flow rate. The steam generator and fuel assembly loss coefficients are biased based on the uncertainty in the loss coefficient correlations. Other pressure losses are decreased to be bounding. Factors such as core bypass flow and steam generator heat transfer are biased to provide a bounding primary coolant flow rate. The following bullet points describe the most significant biases considered in the TH model to calculate the maximum design flow rate:

- Steam generator loss coefficient bias: The best-estimate loss coefficient for the steam generator is decreased by {{ }}2(b),(c),ECI for the maximum design flow calculation. This bias accounts both for error in the loss coefficient correlation, as determined by comparison to test data, and test data measurement uncertainty.

- Fuel assembly loss coefficient bias: {{ }}$^{2(b),(c),ECI}$ uncertainty is subtracted from the overall fuel assembly loss coefficient to bound loss coefficient correlation confidence and experimental uncertainty. The bias value is based on pressure drop testing of a full-size prototype of the fuel assembly.
- Reactor coolant system form loss coefficient bias: For the regions in the RCS loop except for the core and steam generator, the best-estimate form loss coefficients are reduced by {{ }}$^{2(b),(c),ECI}$ for calculation of the maximum design flow. Form loss coefficients for most of the components in the RCS loop are based on empirical correlations. The sum of the SG and core form losses is greater than {{ }}$^{2(b),(c),ECI}$ of the total pressure loss in the RCS loop, making the choice of form loss coefficient elsewhere of less significance.
- Core bypass flow bias: To address uncertainty in the fraction of the total RCS flow rate that bypasses the core, the maximum total bypass flow fraction of {{ }}$^{2(b),(c),ECI}$ of the total RCS flow is used for the maximum design flow conditions.
- Steam generator heat transfer bias: Thermal conductivity of the steam generator tube wall material is decreased by a factor of {{ }}$^{2(b),(c),ECI}$ for the maximum design flow calculation. The primary and secondary side heat transfer coefficients are reduced by {{ }}$^{2(b),(c),ECI}$ for the maximum design flow conditions. Although the TH analysis results show reasonable to excellent agreement with the test data, the tube wall conductivity and the primary and secondary side heat transfer coefficients are biased to cover those unknown differences that may occur between the actual SG performance and the predicted performance.

Note that only the axial flow velocities are calculated in the TH analysis. To determine the cross flow velocities for specific components, it can be conservatively assumed that the cross flow on a component is equal to the calculated axial flow velocity for that component. This method overestimates the forcing function of the vibration. Based on the comparatively low reactor coolant flow rate for the NPM-20 design, this approach is reasonable. For most FIV mechanisms, the free-stream velocity is the required input. Free-stream velocity is the incident velocity before it impacts a susceptible target. However, in the FIV analyses it is typically assumed to be the flow velocity as it passes the target or constriction. The flow area upstream of the constriction is larger than the flow area associated with the constriction; therefore, the average free-stream velocity is lower than the average velocity at the target. While there may be local variations in the free-stream velocity, it is not credible that these variations would occur uniformly at the target face at a velocity higher than the average velocity through the constricted area.

To determine the cross-flow velocities for components subject to a combination of cross-flow and axial flow, since bounding estimates of cross flow velocities can be assumed while still showing acceptable FIV performance, it can be conservatively

assumed that the cross-flow on a component is equal to the calculated total flow velocity for that component. This method overestimates the forcing function of the vibration. Based on the low reactor coolant flow rate, this approach is a conservative estimate that produces acceptable margin.

3.1.2.2 Transient Velocity Analysis

Transient analysis is performed to determine pressures, temperatures, and flow velocities for NPM regions. At lower reactor power levels, natural circulation flow decreases due to the lower heat addition from the core. Based on a review of time-history analyses, there are no normal operating transient responses that result in higher flow rates than are achieved at maximum design full-power conditions. Normal operating transients, such as load following, ramp decreases in reactor power, and reactor trips, result in decreases in flow velocities relative to full-power operating conditions due to the lower heat addition from the core. For conservatism, flow velocities {{ }}$^{2(a),(c),ECI}$ or greater than the maximum design flow value should be used for all FIV mechanisms except for TB and LFI. For TB and LFI, maximum design flow velocities are acceptable.

3.1.2.3 SG Tube Gap Velocity for FEI and VS Evaluations

In accordance with ASME N-1331.1, the flow velocity in the gaps between the tubes is calculated based on the approach flow velocity that would occur if the tubes were not present, multiplied by the ratio of the tube pitch and divided by the pitch minus the diameter. The flow through the SG assembly is dominated by the vertical flow, therefore the radial pitch (distance between two columns) of {{ }}$^{2(b),(c),ECI}$ is more appropriate to use than the axial pitch {{ }}$^{2(b),(c),ECI}$ (vertical distance between the centerlines of two adjacent tubes in the same column). The ratio of the radial pitch divided by the difference between the radial pitch minus the tube outer diameter is equal to {{ }}$^{2(b),(c),ECI}$. This ratio is applied to the approach velocity to calculate the gap flow velocity in both the steam plenum side and feedwater plenum side of the bundle. Note that the approach velocity is based on the maximum design flow rate with a {{ }}$^{2(a),(c),ECI}$ increase in the velocity per Section 3.1.2.2 to bound transient changes in velocity that may be experienced during operating conditions.

3.1.2.4 Velocities Used in Flow-Induced Vibration Analysis

Table 3-4 identifies the methods of obtaining the velocities that are used in the FIV analyses and which flow rate analysis derives them. Bounding flow conditions are used in all analyses. The comparison of test results from thermal-hydraulic test facilities and the TH analysis shows reasonable to excellent agreement. This comparison validates the significant inputs in the TH modeling, such as core and SG form losses and SG performance. In addition, biases are applied per Section 3.1.2.1 to provide a bounding maximum design flow rate. Testing to validate the velocities is not necessary because these FIV inputs have already

been validated with separate effects testing, and bounding maximum design flow velocities are used.

Table 3-4 Flow Conditions Input Summary

Analysis Category	Assumed Conditions	Analysis Method
FEI	Maximum design flow - average velocity	TH
VS	Maximum design flow - average velocity	CFD/TH[Note 1]
AR	Maximum design flow - average velocity	TH
	Maximum CVCS flow - average velocity	TH[Note 2]
F/G	Maximum design flow - average velocity	TH
LFI	Maximum design flow - average velocity	CFD/TH[Note 3]
TB	Maximum design flow - average velocity	CFD/TH[Note 4]

Notes: (1) For the evaluation of VS mechanisms for SG tubes and components exposed to secondary coolant flows, the TH flow is used. CFD analysis is not performed to characterize secondary side flow.

(2) For the evaluation of AR mechanisms for components within piping exposed to primary coolant, the maximum CVCS flow is used.

(3) For the evaluation of LFI mechanism, the TH analysis is used for the bounding flow velocity through pressurizer baffle plate holes.

(4) For the evaluation of TB mechanism, the TH analysis is used for SG tubes and lower SG support while the CFD analysis is used for RVI components

Table 3-5 lists velocities used in the analyses of components subject to FIV. The analysis methods that produce these velocities are identified in Table 3-4, except as noted otherwise below.

Table 3-5 Velocities used in Flow-induced Vibration Analyses

Analysis Category	Component	Velocity (in/s)
FEI Note 1	{{	
VS Note 1		
AR Note 1		
F/G Note 1		
LFI		
		}}2(a),(c),ECI

Table 3-5 Velocities used in Flow-induced Vibration Analyses (Continued)

Analysis Category	Component	Velocity (in/s)
TB	{{	
		}}2(a),(c),ECI

Notes: (1) {{ }}2(a),(c),ECI margin is included in these values for transient velocity changes
(2) Primary side gap velocity based on ASME N-1331.1 are used
(3) For the secondary side, the mixture velocity is used

3.1.3 Damping Ratios

Damping ratio is a necessary input for FEI, LFI, and TB analyses. Damping ratio is also used for VS evaluation of the SG tubes and ICIGTs. Damping can be created from various sources, such as material, fluid viscosity, or structural interactions. Damping reduces a structural response. Damping values may be determined either analytically, through testing, or (for SG tubes) the ASME Boiler and Pressure Vessel Code, Appendix N-1300 (Reference 8.1) values may be used. The following bullet points describe how damping is applied in the FIV analyses:

- Analysis for FEI of SG tubes: damping due to viscous effects of the primary fluid is not credited. Damping created by other sources (material and structural interaction) is expected to be {{ }}2(a),(c),ECI percent based on the guidance in Paragraph N-1331.3 of Appendix N. The damping ratio has a significant influence on the stability ratio that is compared to the acceptance criteria, which represents the margin to the onset of FEI for the SG tubes. Additionally, Regulatory Guide 1.20 states that any attempt to specify structural damping coefficients greater than 1 percent for frequencies greater than seismic frequencies should be supported by experimental measurements. Therefore, prototype testing is

required to confirm that the damping ratio of {{ }}2(a),(c),ECI that is credited in the FEI analyses for the SG tubes is appropriate.

- Analysis for VS: a damping ratio of {{ }}2(a),(c),ECI percent is used for the evaluation of ICIGTs. Prototype testing is planned to confirm the damping ratio of {{ }}2(a),(c),ECI percent that is credited in the VS analysis for the SG tubes.
- Analysis for TB: a damping ratio of {{ }}2(a),(c),ECI percent is used for the SG Alloy 690 tubes and {{ }}2(a),(c),ECI percent is used for all the RVI structures and the lower SG support. These damping ratios {{

  }}2(a),(c),ECI

  Compared with the FEI and VS analyses, a smaller damping ratio is assumed for the SG tubes because lower amplitudes of vibration with less tube-to-tube support interactions are expected with this source of flow excitation. This guidance is consistent with Appendix N-1300. Because the damping values used in TB analysis are {{

  }}2(a),(c),ECI, they are considered to be sufficiently bounding. It is not credible that this input could have a non-conservative effect on the calculated margin of safety. Therefore, testing is not required to verify the damping values used in TB analyses.
- Analysis for LFI: in this assessment, material and structural damping are neglected. Hydrodynamic damping is calculated as a function of the annular gap velocity, and leakage flow instability onset occurs at the velocity when the total damping becomes zero. Neglecting material and structural damping is conservative as this reduces the total system damping.

- Damping due to viscous fluid trapped in the annular space: If a tube is centered in a fluid-filled annulus, the damping is a function of the ratio of the diameter of the fixed outer cylinder to the tube diameter. The damping increases rapidly as the outer boundary approaches the tube. This effect is called a squeeze film. The increased damping due to the squeeze film effect is considered at the {{

  }}2(a),(c),ECI

3.2 Analysis Program Methods and Results

3.2.1 Fluid Elastic Instability

Fluid-elastic instability is a phenomenon primarily associated with arrays of closely packed circular cylinders, such as an SG tube bundle. Instability occurs when during one vibration cycle, the energy absorbed from the fluid exceeds the energy dissipated by damping. Fundamentally, FEI is a strongly coupled fluid-structure interaction mechanism, where the motions of individual cylinders result in fluid force components that are proportional to cylinder displacements and in-phase with the induced velocity of the cylinders. Instability of the SG tube array may occur if the energy input to the SG tubes from fluid force exceeds the energy dissipated by damping. Based on the

strong coupling, once the onset of FEI occurs (i.e., critical fluid velocity is exceeded), vibration amplitudes increase exponentially with additional increase in fluid velocity. Vibration amplitudes are only limited by tube-to-tube contact. The FEI phenomenon occurs in components with the characteristics summarized in Table 2-3. Components susceptible to FEI are indicated in Table 3-1. The helical SG tubing is the only component that is susceptible to FEI.

Evaluation of FEI for typical nuclear straight and U-tube SGs is based on the use of the Connors' equation, which is used to bound the design data captured in Figure N-1331-4 of ASME BPVC, Section III, Appendix N-1300 (Reference 8.1). The Connors' equation is used to determine the reduced critical velocity for the onset of FEI. Based on the reduced critical velocity, a stability ratio (ratio of actual reduced velocity to reduced critical velocity) is calculated and compared with required margins.

An FEI analysis of the inner, middle and outer SG tube columns is performed to demonstrate the margin to the critical velocity throughout the tube bundle. Two tubes within each column are used to bound the range of frequencies possible for each column, and both fixed and sliding boundary conditions are considered. The reduced pitch velocities are computed using the cross-flow component of the primary flow normal to the tube and the translational mode shapes per Equation 82 of N-1331.2 of Reference 8.1, recognizing that mode shapes for the lower frequencies are dominated by axial and torsional motions. The reduced velocity is calculated for each mode using Equation 3-1.

$$\frac{U_i}{f_i D} \geq C\left(\frac{m'(2\pi\xi)}{\rho D^2}\right)^a \qquad \text{Equation 3-1}$$

$$and\ U_{i,r} = \frac{U_i}{f_i D},\ U_{crit} = C\left(\frac{m'(2\pi\xi)}{\rho D^2}\right)^a$$

where:

U_i = mode shape weighted mean pitch velocity for mode i (in/s)

D = outside diameter of cylinder composing the array (in)

f_i = modal frequency (Hz)

ρ = primary fluid density (lb_m/in^3)

ξ = damping ratio (-)

m' = total mass per unit length including hydrodynamic mass (lb_m/in)

C = Connors' coefficient from flow test data (-)

a = exponent from fitting flow test data (-)

$U_{i,r}$ = reduced pitch velocity for mode i (-)

U_{crit} = reduced critical velocity (-)

Bounding Connors' equation values are used to provide conservative values for the critical velocity (i.e., lowest velocity) based on experimental results in Chen (Reference 8.22), and Appendix N-1330 of the ASME code. The critical velocities associated with mass damping values in the NPM-20 operating range are considerably lower than experimental instability points, since the Connors' coefficients provide for fitting of stability results up to mass damping values above 100. A curve fit of {{ }}$^{2(a),(c),ECI}$ is recommended to bound the lowest results of testing data, and to better fit and bound the shape of the data in the lower mass damping range that is applicable for the SG design with mass damping {{ }}$^{2(a),(c),ECI}$

The FEI analysis results show the maximum reduced velocity, a dimensionless number determined for comparison against the critical velocity, is {{ }}$^{2(b),(c),ECI}$ for column 21 and {{ }}$^{2(b),(c),ECI}$ for column 1. Column 21 provides the most limiting reduced velocity results, since this column in the assembly has the longer span lengths between tube supports and the correspondingly lower natural frequencies. The minimum reduced critical velocity is {{ }}$^{2(b),(c),ECI}$ for the steam region, and {{ }}$^{2(b),(c),ECI}$ for the FW region. The FEI reduced velocity results provided in Table 3-6 are plotted in Figure 3-18.

Even for the most limiting SG tube location, positive margin to the FEI acceptance criteria and the predicted onset of FEI is provided. However, due to the prototype classification of the design, the significant analysis inputs and margin of safety are verified by testing because the margin of safety is less than 100 percent for the outermost columns in the SG.

Table 3-6 Fluid Elastic Instability Reduced Critical Velocities and Safety Margins for Connors' Constants of {{ }}$^{2(a),(c),ECI}$

Column, Boundary Condition and Tube	Limiting Frequency (Hz)	$U_{i,r}$Steam Region	Safety Margin Steam Region	$U_{i,r}$FW Region	Safety Margin FW Region
Column 21 Fixed Tube A	{{				
Column 21 Fixed Tube B					
Column 21 Sliding Tube A					
Column 21 Sliding Tube B					
Column 11 Fixed Tube A					
Column 11 Fixed Tube B					
Column 11 Sliding Tube A					
Column 11 Sliding Tube B					}}$^{2(b),(c),ECI}$

Table 3-6 Fluid Elastic Instability Reduced Critical Velocities and Safety Margins for Connors' Constants of {{ }}2(a),(c),ECI

Column, Boundary Condition and Tube	Limiting Frequency (Hz)	$U_{i,r}$Steam Region	Safety Margin Steam Region	$U_{i,r}$FW Region	Safety Margin FW Region
Column 1 Fixed Tube A	{{				
Column 1 Fixed Tube B					
Column 1 Sliding Tube A					
Column 1 Sliding Tube B					}}2(b),(c),ECI

Note 1: This frequency represents a feedwater transition mode that has sufficient displacement in the helical region to not screen out of the FEI assessment and provides a slightly higher reduced velocity than the helical bending mode for column 1 and column 11.

3.2.2 Vortex Shedding

VS is a natural phenomenon that can occur when a bluff body exposed to cross-flow disrupts the flow and creates vortices that shed alternatively from opposite ends of the body, resulting in an alternating force applied to the body. When the frequency of the VS force is at or near the natural frequencies of the body, a "lock-in" phenomenon occurs: the body experiences resonance, resulting in large oscillations, potentially leading to rapid component degradation and failure due to low cycle fatigue. To determine if VS is a concern, the natural frequencies of the component of interest need to be compared to its VS frequency. The VS phenomenon occurs in components with the characteristics summarized in Table 2-3. Components susceptible to VS are indicated in Table 3-1.

For components other than the upper riser bellows, the VS susceptibility evaluation is performed using the method in Subsection N-1324.1 of the ASME BPVC Section III (Reference 8.1). The VS analysis is divided into three parts. The first part of the analysis determines the natural frequencies of the components. This task is performed either by hand calculation or FEA, depending on the complexity of the component. The second part of the analysis evaluates the components for VS lock-in susceptibility using the four criteria in Subsection N-1324.1 of the ASME BPVC Section III (Reference 8.1). The final section calculates the safety margin to the onset of VS for each component.

For the upper riser bellows, the bellow natural frequencies are calculated per the equations in Section III of Reference 8.26. The bellow natural frequencies are then compared to the upper and lower VS frequencies, which are based on the Strouhal numbers in the range of 0.1 to 0.3 per experimental results (Reference 8.26) to evaluate the VS susceptibility of the bellows.

Table 3-7 summarize the VS evaluation results for the components other than GTs, SG tubes, and upper riser bellow. The results show that over 100 percent margin is demonstrated for the thermowells, lower SG support, CRD shaft sleeve, CRD shaft supports, CRAGT support plate, CRD shaft support, and RCS injection RVI. Note that

the results for the RCS hot thermowells can be conservatively applied to support blocks since the thermowells are significantly more flexible, have a smaller characteristic dimension, and are exposed to a lower primary coolant flow velocity. Similarly, the results of the CRAGT and CRD shaft supports bound the performance of the upper and lower core plates, since they are more flexible, have smaller characteristic dimensions, and experience similar primary coolant flow velocities. Additionally, the upper and lower core plates do not have unobstructed flow paths downstream of the portion of the component experiencing cross flow, which makes the likelihood of generating a coherent vortex improbable.

Table 3-7 Results of VS Analysis for Components other than Guide Tubes, SG Tubes, and Upper Riser Bellows

Component	Fundamental Natural Frequency (Hz)	Characteristic Dimension (in)	Flow Velocity (in/s)	Safety Margin (%)	Passing Criteria(Note 1)
RCS Thermowell - hot region	{{				
RCS Thermowell - cold region					
Thermowell - MS					
Thermowell - FW					
Lower SG Support					
CRD Shaft Sleeve					
Lower CRD Shaft Support					
Intermediate CRD Shaft Support					
Top CRD Shaft Support					
CRAGT Support Plate					
CVCS Injection RVI (downcomer)					}}2(a),(c),ECI

Notes:

(1) Passing criteria A and D refer to the criteria in Method (a) and (d) of Subsection N-1324.1 of the ASME BPVC Section III, respectively. Method A criteria requires that the reduced velocity, which is calculated as the flow velocity divided by the product of the fundamental natural frequency times the characteristic length, be less than 1.0. Method D criteria requires that the structural resonance frequency be at least 30 percent removed from the vortex shedding frequency, which is calculated based on the Strouhal number determined from Figure 3-3 of Reference 8.3 using the Reynolds number. When using Method D, the vortex shedding frequency in the drag direction, which is twice the vortex shedding frequency, is also considered in the margin calculation as required by the Code.

(2) For lower and intermediate CRD shaft supports, the Strouhal number determined from Figure 3-3 of Reference 8.3 is {{ }}2(a),(c),ECI.

Table 3-8 summarizes the results for the ICIGTs, {{

}}2(a),(c),ECI. The reported safety margins are the maximum of method B and C results. Method (b) states that lock-in is avoided if reduced damping is greater than 64. Method (c) states that lock-in is avoided if the reduced velocity, which is calculated as the flow velocity divided by the product of the fundamental natural frequency times the characteristic length, is less than 3.3 and the reduced damping is greater than 1.2. The reduced damping is calculated using the method provided in Subection N-1324.1 (b) of Reference 8.1. The reduced velocity and reduced damping are calculated for each of the first nine modes. The results show that over 100 percent margin is demonstrated. The reduced damping for {{

}}2(a),(c),ECI

Table 3-8 Results of VS Analysis for ICIGTs

Mode	Frequency (Hz)	Reduced Velocity	Reduced Damping	Passing Criteria	Safety Margin
{{					
					}}2(a),(c),ECI

An assessment of the SG tubes is performed using N-1324.1 Methods A, B, and C which are the three methods in the Code that are applicable to tube bundles. Modal analysis of the SG tubes is performed using ANSYS. The ANSYS model considers two possible boundary conditions at each support location: fixed or sliding conditions. Three columns, Column 1, 11, and 21, which represent the innermost, middle, and outermost tube columns, are analyzed. The model for each column contains the two bounding tubes: the top most tube (Tube B) and the bottom most tube (Tube A). Modes are analyzed for each of the three columns up to a natural frequency of 300 Hz. Additional discussion of the SG tube modal analysis is provided in Section 3.1.1.1.

The VS analysis of SG tubes is performed for the two regions that are susceptible to the VS lock-in: the steam transition region and the feedwater region. The tube sections in the steam transition region represent the first several rows of the tube bundle. Section N-1344 of Reference 8.1 indicates that only the first several rows of a tube bundle are at risk of VS lock-in. The tube sections in the feedwater region analyzed for VS lock-in are the portion of the tubes that are exposed to cross flow without downstream obstruction to preclude vortex shedding.

Results for the SG tube VS analysis demonstrate a margin over 100 percent for all modes of the SG tubes per Table 3-9. Note that Method (a) of N-1324.1 conservatively uses the vortex shedding frequency for the Strouhal number equal to 1.0. {{

}}2(a),(c),ECI

Table 3-9 Results of VS Analysis for SG Tubes

Column-Tube	Boundary Condition at Tube Support	Region	Frequency (Hz)	Reduced Velocity	Reduced Damping	Passing Criteria	Safety Margin St=1	Safety Margin {{ }}2(a),(c),ECI
{{								
								}}2(a),(c),ECI

The natural frequency of the upper riser bellows on the riser and downcomer side is calculated and compared to the VS frequency range per the method in Reference 8.26. The bellows consist of a series of convolutions that can act as a bluff body, which protrudes into the axial flow in both the downcomer and riser side. The VS lock-in susceptibility evaluation is performed for both the downcomer and riser side, and the results are summarized in Table 3-10. The results demonstrate margins over 100 percent.

Table 3-10 Upper Riser Bellow VS Results

Side	First Mode Natural Frequency	Highest Mode Natural Frequency	Lower VS Limit Frequency	Upper VS Limit Frequency	Safety Margin
Downcomer	{{				
Riser					}}2(a),(c),ECI

3.2.3 Turbulent Buffeting

Based on flow rates needed to achieve desired thermal performance for industrial heat transfer applications (e.g. power plants), turbulence is an inevitable consequence. Coupling between a structure and the random pressure fluctuations induced by turbulent flow is typically weak. The amplitude of the structural response is a function of several variables, including the turbulent forcing function and the frequency of the structure. Components that are subject to turbulent flow are susceptible to turbulent vibration. Additionally, a component interface location that may not be directly subject to turbulent flow but is in the load path of one or more components that are subject to turbulent flow is also susceptible to turbulent vibration.

Although the random vibration due to TB is of much smaller amplitude than that experienced in FEI or VS, it is important because it exists whenever there is turbulent flow over a susceptible component. Turbulent buffeting vibration can be induced in parallel flow, axial flow, or cross-flow. Turbulence-induced vibration occurs due to a fluctuating pressure in the flow. The fluctuating pressure is quantified by a forcing function, which is characterized by its power spectral density (PSD) and correlation function. Three significant parameters are needed to characterize the PSD and correlation function: convective velocity, correlation length, and the PSD.

The convective velocity, as implemented in the coherence function, describes the phase relationship of the forcing function at two points on the surface of the structure. From a physical standpoint, the convective velocity is the velocity at which eddies are swept downstream, thus causing a phase shift in the fluctuating pressure between two points. Based on literature review, convective velocity can be a maximum of the free-steam velocity and a minimum of 0.5 times the free-stream velocity for parallel or axial flow. The limiting convective velocity within the range is selected when evaluating the coherence function.

The correlation length is equivalent to the scale of the largest turbulent eddy, which is a measure of the longest distance over which the velocity at two points of the flow field is correlated. For each component, the flow is characterized as parallel, cross, two-phase, or axial, and the characteristic length is determined. A bounding correlation length range is determined based on literature review. Similar to the convective velocity, the range of correlation lengths is evaluated to ensure a bounding value is selected for each component forcing function.

The PSD is determined to support characterization of the forcing function. The PSD as applied to flow-induced turbulent response refers to the energy distribution of a variable as a function of frequency. Many RVI components can be approximated as cylinders in cross flow or annular flow. For these idealized arrangements, bounding PSDs based on literature are used. Table 3-11 summarizes the PSD types that are applied to components susceptible to TB. The overall analytical uncertainty for the SG tubes is judged to be the highest relative to other susceptible components; therefore, prototype testing is performed to verify the adequacy of the PSDs used for the SG tubes.

The methodology for determining the structural response spectra due to turbulent buffeting is based on the acceptance integral methodology. First ANSYS is used to run a modal analysis on the structural model. This information provides the required structural properties. The loading on the structure is applied using pressure PSDs. The spatial distribution of the PSDs are characterized by a coherence function. With the mode information, pressure PSDs, and coherence functions, the acceptance integrals are calculated. The acceptance integrals represent the contribution to the response from different mode combinations.

In the TB evaluations, the vibration amplitude is not calculated for components with a first mode frequency greater than 200 Hz because vibration amplitudes are insignificant with high structural frequencies. Components with lower first mode frequencies experience higher root mean square (RMS) vibration amplitudes. Vibration amplitude is also not determined for components that based on flexibility and flow conditions can be shown to be bounded by the analyzed components. By design, supports are thicker and less flexible than the components they support; hence, the component is analyzed for turbulent buffeting vibrations. The results generally bound the performance of the support. Therefore, no PSD is specified in Table 3-11 for certain components identified as susceptible to TB in Table 3-1.

Table 3-11 Turbulent Buffeting Power Spectral Density Inputs used in Analysis

Flow Type and Component Shape (Note 3)	Applicable Components	Literature PSD Used
Single-phase axial flow for tubes	{{	Equation 3-3
Two-phase axial flow for tubes		Equation 3-4, Equation 3-5, Equation 3-6, Equation 3-7
Tube bundle cross-flow		Equation 3-8
Bounding annular flow	}}2(a),(c),ECI	Equation 3-2

Note 1: The RVI assembly is a collection of structures that responds to turbulent buffeting forces as a group. It includes the {{ }}2(a),(c),ECI

Note 2: Is applied to the {{ }}2(a),(c),ECI

Note 3: A PSD of zero is used for the sections of ICIGT and CRD shafts in the PZR, and the section of the CRD shafts in the CRD shaft sleeve above the highest CRD shaft support.

Note 4: PSD applied for the portion of the {{ }}2(a),(c),ECI

Equation 3-2 is from Reference 8.2. It provides a PSD for components with annular flow velocities. It is applied to some components that experience cross-flow, and this simplification is bounding based on the frequencies and characteristic lengths of the analyzed components. Due to the relatively low flow velocities, the reduced frequency for some components is larger than five. For those cases, the PSD uses the third part of Equation 3-2 which reduces the magnitude of the PSD with frequency at a conservatively slow rate. The second and third parts of Equation 3-2 are equal when the reduced frequency is five.

$$G_p(f) = \rho^2 v_f^3 R_h 0.155 e^{-3.0F} \quad , 0 < F < 1$$
$$G_p(f) = \rho^2 v_f^3 R_h 0.027 e^{-1.26F} \quad , 1 < F < 5 \qquad \text{Equation 3-2}$$
$$G_p(f) = \rho^2 v_f^3 R_h 0.000135 e^{-0.2F} \quad , \; F > 5$$

where:

$G_p(f)$ = PSD of the turbulent pressure as a function of modal frequency (psi^2/Hz),

ρ = Fluid density (lbf-s^2/in^4),

v_f = Free-stream velocity (in/s),

R_h = Hydraulic radius (in), and

F = Reduced frequency (-).

The test data from Chen (Reference 8.12) are used to characterize a PSD for axial flow over tubes. The relationship is applicable to low Strouhal numbers.

$$G_p(f) = 0.000002720 \rho^2 v_f^3 2R_h S^{-0.25} \quad , 0 < S \leq 5$$
$$G_p(f) = 0.0002275 \rho^2 v_f^3 2R_h S^{-3} \qquad , 5 < S \leq 10 \qquad \text{Equation 3-3}$$

where:

$G_p(f)$ = PSD of the turbulent pressure as a function of modal frequency (psi^2/Hz),

ρ = Fluid density (lbf-s^2/in^4),

v_f = Free stream velocity (in/s),

R_h = Hydraulic radius (in), and

S = Strouhal number (-).

For the two-phase region, the correlations by Giraudeau from Reference 8.20 are implemented. These correlations are force PSDs of two-phase fluids around 90° elbows. Giraudeau found that the force PSD on an elbow is caused by the changes in the mass flux through the tube due to turbulent two-phase flow. The helical tube experiences similar behavior in the two-phase region.

The Giraudeau correlations are based on Equations 17, 19, 20, and 21 from Reference 8.20, repeated in Equation 3-4, Equation 3-5, Equation 3-6, and Equation 3-7. The five empirical constants that go into the Giraudeau PSD are defined in Table 1 of Reference 8.20 and repeated in Table 3-12. The constants are defined for four void fractions. When the actual void fraction in the tube is between the tabulated values, linear interpolation is used. As a two-phase PSD, the Giraudeau correlation is only used when the void fraction is between 0.05 and 0.95. These limits are selected based on the range of void fractions used in the test data that support the Giraudeau correlation. Note that there is a typo in Table 1 of Reference 8.20 for k_2 at a void fraction of 0.95. The typo is corrected in Table 3-12 and in the associated calculations.

The Giraudeau PSD is a force PSD on a 90-degree elbow. To convert the force PSD to a pressure PSD, it is divided by the area of the element squared. Also, each element only sweeps out a portion of a 90-degree bend. Therefore, the PSD is also multiplied by the square root of one minus the cosine of the angle swept out by the element. This factor ensures that the sum of all force vectors on elements that make up a 90-degree bend sum to the appropriate value. The Giraudeau PSD is for flow around an elbow and is therefore, only applied radially on the tube. The single-phase PSD is also applied in the two-phase region. The single-phase PSD is insignificant compared to the Giraudeau PSD in the radial direction, but provides excitation in the vertical direction.

$$\bar{f} < \bar{f}_0 \qquad \overline{\Phi} = k_1 \bar{f}^{m_1}$$
$$\bar{f} \geq \bar{f}_0 \qquad \overline{\Phi} = k_2 \bar{f}^{m_2} \qquad \text{Equation 3-4}$$

$$\overline{\Phi} = \frac{\Phi}{\left(\rho_l j^2 D_h^2\right)^2} \frac{j}{D_h} We^{0.8} \qquad \text{Equation 3-5}$$

$$\bar{f} = \frac{f D_h}{j} \qquad \text{Equation 3-6}$$

$$We = \frac{\rho_l j^2 D_h}{\sigma} \qquad \text{Equation 3-7}$$

where:

$\bar{f}$ = Reduced frequency (-)

$\bar{f}_0$ = Reduced frequency of maximum force

$\bar{\Phi}$ = Normalized force PSD (-)

Φ = Force PSD (lbf^2/Hz)

f = Frequency (Hz)

D_h = Hydraulic diameter (in)

ρ_l = Liquid density ($lbf\text{-}s^2/in^4$)

j = Mixture velocity (in/s)

We = Weber number (-)

σ = Surface tension (lbf/in)

k_1 and k_2 = Correlation factor (-)

m_1 and m_2 = Correlation exponent (-)

Table 3-12 Giraudeau Power Spectral Density Correlation Empirical Constant

Void Fraction	$\bar{f}_0$	k_1	k_2	m_1	m_2
0.25	0.050	3.644e4	2.234	1.39	-1.84
0.50	0.058	3.466e7	0.460	3.31	-3.06
0.75	0.040	8.866e8	0.492	3.43	-3.19
0.95	0.018	7.105e9	0.004[1]	3.58	-3.44

Note 1: Reference 8.20 contains a typo in Table 3-12. The value of 0.040 is corrected to 0.004 here. The correct value can be verified by comparing the calculated PSD using the k_1 and k_2 functions at $\bar{f}_0$.

A PSD to represent cross-flow over a tube bundle geometry is specified in Equation 3-8. This equation is from Reference 8.2 and is expected to provide bounding results for the frequency range, flow velocities, and SG tube diameter of the NuScale SG tube bundle. As mentioned previously, this assumption is verified by testing.

$$G_p(f) = 0.5\rho^2 v_f^3 R_h 0.01 \qquad 0 < \mathrm{F} < 0.1$$

$$G_p(f) = 0.5\rho^2 v_f^3 R_h 0.02 \qquad 0.1 \le F < 0.4 \qquad \text{Equation 3-8}$$

$$G_p(f) = 0.5\rho^2 v_f^3 R_h 0.00053 F^{-3.5} \qquad F \ge 0.4$$

where:

$G_p(f)$ = PSD of the turbulent pressure as a function of modal frequency (psi^2/Hz)

ρ = Fluid density (lbf-s^2/in^4)

v_f = Free stream velocity (in/s)

R_h = Hydraulic radius (in)

F = Reduced frequency (-).

The structural response due to the turbulence is calculated using the inputs discussed. The modal analysis results for RVI components are provided in Figure 3-7 to Figure 3-11. Equations to determine the RMS response are assigned based on the direction of the flow and the dimension of the structure, using the appropriate PSDs, damping ratios, modal analysis results, and flow characteristics for the analyzed components. Equation 8.45, Equation 8.46, and Equation 8.47 of Reference 8.2 are the basis for the mean square response calculation. {{

}}$^{2(a),(c),ECI}$ Using the RMS response, degradation mechanisms associated with impact and vibration fatigue are evaluated. For the structures where the support (i.e., RVI assembly) and the structure may move independently, the relative motion is calculated by adding the two vibrations together with a square root of the sum of the squares method. Components with fundamental frequencies less than 200 Hz and those whose response cannot be bounded by nearby components exposed to similar turbulent conditions are evaluated for fatigue.

Figure 3-7 CRAGT first mode at {{ }}2(a),(c),ECI

{{

}}2(a),(c),ECI

Figure 3-8 CRDS first mode at {{ }}2(a),(c),ECI

{{

}}2(a),(c),ECI

Figure 3-9 Lower ICIGT first mode at {{ }}2(a),(c),ECI

{{

}}2(a),(c),ECI

Figure 3-10 Upper ICIGT first mode at {{ }}2(a),(c),ECI

{{

}}2(a),(c),ECI

Figure 3-11 Injection line, riser first mode at {{ }}2(a),(c),ECI

{{

}}2(a),(c),ECI

Table 3-11 lists the components analyzed for turbulent buffeting. Each has a fundamental frequency below 200 Hz. After the RMS response is calculated as discussed above, components undergo further separation screening: the acceptance criterion for a component remaining separated from an adjacent component is that the clearance is greater than 5 times the RMS deflection. For components that do not meet the criterion, the surface stress is calculated and an impact fatigue assessment is performed.

The impact stress is estimated using the empirical approximation shown in Equation 3-9 (Reference 8.2). The crossing frequency is used as the impact frequency.

$$S_{rms} = c\left(\frac{E^4 M_e f_c^2 y_{max}^2}{D^3}\right)^{1/5} \qquad \text{Equation 3-9}$$

where:

S_{rms} = Surface stress due to impact (psi)

c = Contact stress parameter, page 357 of Reference 8.3 (-)

E = Elastic modulus (psi)

M_e = Effective mass, for a tube usually taken as 2/3 of the mass of the two adjacent spans (lbf-s^2/in)

f_c = Crossing frequency (Hz)

y_{max} = Maximum RMS vibration amplitude (in)

D = Tube outer diameter (in)

An alternating impact stress is calculated as one-half of the surface stress, and used with a fatigue curve based on RMS stress (similar to Figure 11.6 of Reference 8.2) to obtain a usage factor. In addition to the impact fatigue, TB can cause fatigue due to vibration stresses. However, due to the very low vibration amplitudes and alternating stresses, the vibration stresses do not result in fatigue usage for components susceptible to TB.

The modal results are used to calculate the maximum RMS vibration amplitude and the crossing frequency. Table 3-14 lists the amplitudes and crossing frequencies for the RVI components.

Table 3-13 Maximum RMS Vibration Amplitude and Crossing Frequencies

Component	Max. RMS Vibration (in)	Crossing Frequency (Hz)
CRAGT Outer Diameter	{{	
CRD Shaft		
Lower ICIGT		
Upper ICIGT		
RVI Assembly		}}2(a),(c),ECI

As an example, Figure 3-12, Figure 3-13, and Figure 3-14 show the results for the upper ICIGT. Figure 3-12 shows the mode shapes in the X direction (radial) for the first eight modes. The mode shapes are zero at the supports and maximum at the approximate mid-spans. Figure 3-13 shows the structural response (Note the X and Z direction response are equal). The peaks are at the modal frequencies. Figure 3-14 shows the RMS vibration amplitude as a function of vertical position. {{

}}2(a),(c).ECI

Figure 3-12 Upper ICIGT X Direction Mode Shapes

{{

}}2(a),(c),ECI

Figure 3-13 Upper ICIGT Structural Response PSD

{{

}}2(a),(c),ECI

Figure 3-14 Upper ICIGT RMS Vibration as a Function of Position

{{

}}2(a),(c),ECI

A subset of the RVI components are analyzed for impact stress calculations. Those components include the CRAGT on the CRAGT support, the CRD shaft impact on the alignment cone, the upper ICIGT impact on the second highest CRD shaft supports, and the lower ICIGT impact on the upper core plate. Component pairs with small amplitude vibrations and large clearances are not included: the RVI assembly, which has a {{ }}2(a),(c),ECI clearance between the RPV and the upper core support blocks is an example. For the ICIGT, CRAGT, and the CRD shaft, impact stress calculations, a contact stress parameter based on five times the RMS value is used because this is the furthest from the support that the shaft could be while still regularly having impacts.

Table 3-14 Reactor Vessel Internals Impact Stress Calculations

Quantity	CRD Shaft	Lower ICIGT	Upper ICIGT	CRAGT
{{				
				}}2(a),(c),ECI

The fatigue due to impact stresses is evaluated. Since the magnitude of the impact stresses are relatively small, the number of allowable cycles is extremely large, resulting in negligible usage values (i.e., low amplitude high cycle fatigue). Table 3-15 provides the results for the RVI components.

Table 3-15 Reactor Vessel Internals Impact Fatigue Calculations

Quantity	CRD Shaft	Lower ICIGT	Upper ICIGT	CRAGT
{{				
				}}2(a),(c),ECI

The SG tube modal analysis from Reference 3.1.1.1 is used for the TB assessment of the SG tubes. {{

}}2(a),(c),ECI The stress distribution is shown in Figure 3-15. Figure 3-16 shows the stress response at the location with the largest RMS value.

The maximum total RMS vibration amplitude from {{

}}2(a),(c),ECI

Figure 3-15 Column 21 Tube B RMS Stress

{{

}}2(a),(c),ECI

Figure 3-16 Column 21 Tube B Stress Response PSD at Maximum Location

{{

}}2(a),(c),ECI

The modal analysis of the lower SG support shows that there are only four modes within the frequency range of interest. There are {{

}}2(a),(c),ECI. The RMS displacement at the end is small enough, {{ }}2(a),(c),ECI compared to the clearances required to assemble the SG that imp t ear does not need to be considered.

The stress response due to TB is plotted in Figure 3-17. The RMS bending stresses are {{ }}2(a),(c),ECI. These stresses are below the RMS endurance limit for fatigue.

Figure 3-17 Lower SG Support Stress Response PSD at the Fixed End

{{

}}2(a),(c),ECI

Modal analysis of the IFR is performed to determine if the frequency is low enough to warrant assessment of turbulent buffeting loads. {{

}}2(a),(c),ECI The cantilevered length is less than {{ }}2(a),(c),ECI and has a relatively large cross sectional moment of inertia to resist bending. The IFR first mode frequency is approximately {{ }}2(a),(c),ECI than 200 Hz. Due to the stiffness of the IFR, turbulent buffeting loads do not require assessment regardless of the flow conditions, which may be single-phase, two-phase, or reverse flow.

3.2.4 Acoustic Resonance

When energy within a fluid is changed, either potential or kinetic, there is a potential for an acoustic wave to be generated. Acoustic waves can be generated from heat transfer, pump operation, vortex shedding, phase change, and pressure drop across geometry. In specific geometries, the acoustic wave is generated at a frequency that coincides with a natural acoustic frequency of the confining structure, resulting in resonance and significant pressure fluctuations throughout the acoustic volume of the confining structure.

Components susceptible to AR are indicated in Table 3-1. The steam plenums could be subject to internal acoustic resonance; however, acoustic excitation is not expected in the steam plenum from the SG tube exit because there is significant turbulence and it is unlikely that vortices develop in this region. The MSIVs are an unlikely source of pressure fluctuations associated with AR because the MSIVs are directly mounted on the steam piping with no standpipe, and there is little disruption of the flow inside the MSIVs. The SG inlet flow restrictors are designed to limit DWO inside the SG tubes. The {{ }}$^{2(a),(c),ECI}$ and are screened from further evaluation.

The locations that flow excitation due to AR may be possible are at the branch lines and cavities at the following locations:

- DHRS condensate piping to SGS feedwater line
- Component and instrument ports
  - RRV
  - Ultrasonic flowmeter cavities
- RCS injection line to ECCS reset line
- CNTS CVC drain valve branch
  - Injection
  - Discharge
  - Pressurizer spray
  - RPV high point degasification
- SGS pressure relief valve branch
- CNTS FW drain valve branch

To determine if there is a concern for AR, the piping locations where this source of flow excitation is possible are identified and the Strouhal number is calculated for each location. To determine the margin to AR, the calculated Strouhal number is compared to the critical Strouhal numbers that could lead to the onset of AR. As documented in Reference 8.18, Figure 17, experiments show that the critical Strouhal number at the onset of resonance is dependent on the local geometric parameters including the ratio of the branch and main pipe diameters (d/D) as well as the ratio of

the nearest upstream flow disturbance to the main pipe diameter, (x/D). Table 3-16 shows critical Strouhal numbers for each location, which are the first-order Strouhal numbers. The second-order critical Strouhal number is twice the first-order Strouhal numbers.

Table 3-16 NuScale Critical Strouhal Numbers

Location of Component	x/D	d/D	Strouhal Number
DHRS condensate line to SGS feedwater line	{{		
Component and instrument ports: ultrasonic flowmeter			
Component and instrument ports: RRV			
RCS injection line to ECCS reset line			
CNTS RPV high point degasification drain valve branch -with nitrogen[1]			
SGS pressure relief valve branch			
CNTS FW drain valve branch			}}2(b),(c),ECI

Notes: (1) For the CVCS drain valves, only the Strouhal number for the degasification line containing nitrogen gas number is presented because all other drain and vent valve locations have higher margin based on calculated drain valve Strouhal values. Nitrogen gas flows into and out of the pressurizer, depending on the evolution being performed. The case of in-flow provides a smaller x/D and thus higher, more limiting critical Strouhal number.

(2) As described in Reference 8.18, branch connections located on the same side of the flow path as the inner radius of the upstream bend behave as if the bend were infinitely far upstream.

(3) This connection is a cross. The flow splits and half of the flow turns away from the DHRS condensate line dead leg. The value of {{ }}2(a),(c),ECI, the maximum value from the experimental data, is used here.

The safety margin is determined by comparing the critical Strouhal number to a minimum component Strouhal number calculated at maximum flow conditions for each region. The component Strouhal number is higher at lower flow velocities and is thus bounded by the results at the maximum flow conditions. Positive margin to the critical Strouhal number indicates that the region would not be exposed to an onset of AR at an intermediate flow condition. Safety margin results for first order shear layer mode excitation are summarized in Table 3-17. The results demonstrate over 100 percent margin for the first order Strouhal number at all the locations, which results in a positive second order Strouhal number safety margin. Therefore, no additional testing for acoustic resonance is recommended for these components.

Table 3-17 Acoustic Resonance Results Summary

Branch Description	Strouhal Number	First-Order Critical Strouhal Number	First-Order Safety Margin	Second-Order Critical Strouhal Number
{{				
				}}2(a),(c),ECI

Note:
(1) Of the CVCS drain valves, the degasification line containing nitrogen bounds other drain and vent valve locations, with the smallest safety margin.

3.2.5 Leakage Flow Instability

When fluids flow through a thin space with at least one flexible boundary, the flow can cause instability resulting in vibration of the flexible wall. This phenomenon is referred to as leakage flow instability (LFI) and is driven by the potential energy stored in the static fluid pressure. The LFI phenomenon occurs in components with the characteristics summarized in Table 2-3. Section 2.3.8 provides a discussion of the LFI screening evaluation. No components are susceptible to LFI as indicated in Table 3-1.

3.2.6 Gallop and Flutter

Components with non-circular cross-sections are potentially susceptible to flutter or gallop vibration phenomenon. Galloping is a phenomenon resulting from wake instability typically observed in civil engineering structures with noncircular cross sections. As the fluid medium causes vibration of the structure, the response varies because of the changing orientation and cross-section subject to fluid force and may result in both torsional and lateral galloping. This varying excitation can lead to very large amplitude vibrations. Flutter is a phenomenon similar to galloping, except that the term derives from the aerospace industry as defined to be a coupled torsion-plunge instability of airfoil structures. The lower SG support, as indicated in

Table 3-1, is the only NPM structure that requires evaluation for flow excitation created by gallop and flutter.

The torsional oscillations of bluff sections are sensitive to the vortices generated downstream of the rotating structure. The most reliable approach to account for the unsteady and coupled vortex effects on non-circular sections is to scale test results performed on similar designs. Flow tests of rectangular cross sections have been performed to investigate the influence of the VS frequency and the response of the structure to torsional gallop considering both smooth and turbulent flow conditions. The results of the flow test summarized in Reference 8.4 are applicable to rectangular cross sections whose height-to-width ratio is between 0.2 and 5.0. For the lower SG support, this ratio is {{ }}$^{2(a),(c),ECI}$, and the results of these flow tests are applicable. The testing predicts that the critical velocity to the onset of torsional galloping is {{ }}$^{2(a),(c),ECI}$ which is much greater than the maximum primary flow velocity plus six percent margin for transient velocities in this region of approximately {{ }}$^{2(a),(c),ECI}$

Flutter is also precluded for the lower SG support. Because significant separation exists between the bending and torsional frequency of the SG lower tube support ({{ }}$^{2(b),(c),ECI}$), it is not possible for plunge gallop and torsional gallop to become coupled such that the SG lower tube support experiences flutter. Due to the large margins to the onset of these phenomena, no confirmatory testing is required to verify the flutter and gallop analyses.

3.2.7 Thin-Walled Pipe Subject to High Velocity Internal Flow

High velocity flow through a thin-walled pipe has the potential to cause a pipe to buckle or vibrate at unacceptably large amplitudes. The NPM piping is designed to have sufficient wall thickness to meet internal and external design pressure requirements and sufficient support to meet loading requirements; therefore, turbulent flow conditions are not expected to adversely affect the piping.

Table 10-1 of Reference 8.3 identifies piping instability modes due to internal flows as a function of the piping support boundary conditions (clamped, pinned, sliding, or free) and whether the pipe geometry is straight or curved. There are few piping segments in the NPM that are straight. Most contain bends to accommodate routing as well as allow for thermal growth. Piping supports in the NPM are primarily {{ }}2(a),(c),ECI supports. These supports are designed to constrain {{ }}2(a),(c),ECI defined in Table 10-1 of Reference 8.3. NPM piping also contains clamped boundary conditions when it attaches to the RPV or CNV nozzles. There are no supports that provide a pinned boundary condition. A free boundary condition exists in the containment flooding and drain piping, which terminates in the containment atmosphere, and the tubing in CRD system piping assembly. The following instability modes can be ruled out.

- There are no straight pipes with clamped-clamped, clamped-pinned, or pinned-pinned boundary conditions, since there are no piping supports that are pinned and no straight pipes that extend between the RPV and CNV.
- SGS piping contains clamped-clamped boundary conditions, but the piping is curved and therefore not susceptible to an instability mode.
- There are no straight or curved pipes that are clamped-free, except as noted below. Next to each RPV or CNV piping connection is a {{ }}2(a),(c),ECI. The limiting segment for each system is evaluated.
- Containment flooding and drain and CRD systems have a free boundary condition in the piping assemblies. These segments are susceptible to flutter instability.
- As stated above, clamped-sliding boundary conditions exist for most NPM piping. These piping segments are susceptible to flutter instability.

Figure 10-5 of Reference 8.3 is used to assess if flutter is a concern for piping with clamped-sliding boundary conditions. The figure is developed for a simple fluid conveying straight cantilever pipe. {{ }}2(a),(c),ECI.

To determine whether the dimensionless frequencies (Ω) are stable, dimensionless variables related to the velocity in the pipe (Y-axis variable) and the mass of the pipe (X-axis variable) are calculated using Equation 3-10 and Equation 3-11:

$$\beta = \frac{\rho A_{ID}}{M} \qquad \text{Equation 3-10}$$

$$V = vL\left(\frac{\rho A_{ID}}{EI}\right)^{1/2} \qquad \text{Equation 3-11}$$

Where

β = dimensionless constant for cantilever pipe (-)

M = piping mass (pipe plus fluid) per unit length (lb/in)

ρ = fluid density (lb/in^3)

A_{ID} = pipe inner diameter area (in^2)

V = dimensionless constant for velocity (-)

v = flow velocity (in/s)

L = pipe unsupported length (in)

E = modulus of elasticity (psi)

I = moment of inertia of pipe cross-section (in^4)

Since the equations are developed for a straight pipe, {{

}}$^{2(a),(c),ECI}$ in order to more closely match the straight piping basis for these equations.

The limiting piping segments in the {{

}}$^{2(a),(c),ECI}$ are assessed for buckling and flutter instability. Once the dimensionless constants are determined, they are compared to the instability limit in Figure 10-5 of Reference 8.3 to show whether the limiting pipe segment in each system is stable. Dimensionless natural frequencies are shown to be below the unstable region with considerable margin. The highest dimensionless velocity result is {{ }}$^{2(a),(c),ECI}$ for the {{ }}$^{2(a),(c),ECI}$, which is well below the limit of approximately {{ }}$^{2(a),(c),ECI}$ per Figure 10-5 of Reference 8.3. This evaluation demonstrates that no piping instabilities are expected due to turbulent flow.

3.2.8 Comparison to San Onofre Nuclear Generating Station Replacement Steam Generator Issues

The NuScale SG differs from traditional recirculating and once-through SG designs, such as the replacement San Onofre Nuclear Generating Station (SONGS) SGs. Accordingly, the failures experienced with the SONGS replacement steam generators and the consequent lessons learned are considered, but are not directly applicable to the NuScale design.

The NuScale SG supports are discussed in Section 2.3.2. For traditional (and the SONGS replacement) SG design, industry U-bend design practice applied flat bar (anti-vibration bar) supports because of advantages such as decreased tube-to-anti-vibration bar wear rates. However, experience with the SONGS replacement SGs showed that flat bar supports do not adequately restrict in-plane

tube motions. The NuScale SG tube supports are designed to prevent out of plane tube-to-tube wear by separating the tube columns radially, and tube support channels and tabs prevent in-plane tube-to-tube wear by separating the tubes axially. The NuScale SG design also requires small clearances between the SG tubes and tube support column tabs, ensuring that there are contact forces to prevent inactive supports and unacceptable tube-to-tube support wear.

Additionally, the NuScale SG tube wall thickness is thicker than existing SG designs, and the use of Alloy 690 SG tubing mitigates SG corrosion compared to Alloy 600 used in other SG designs. The reactor coolant flow rates in the NPM are an order of magnitude lower than flow rates across the SG in PWR recirculating steam generators, such as the SONGS design. This low flow rate reduces the turbulent flow energy available to cause FIV degradation of the SG tubes.

These SG features are developed based on the SONGS lessons learned and previous industry operating experience, and ensure structural integrity against damage and degradation due to FIV, such as those issues observed with the SONGs replacement SGs.

Fluid elastic instability is a phenomenon that affects the outside of the SG tubes. Gap velocities for SONGS were approximately an order of magnitude higher than in the NuScale design, based on the higher secondary coolant steam flow velocities compared to the NuScale natural circulation primary coolant velocities. Also, based on thermal hydraulic principles, uncertainties in the steam conditions and the resulting impact on the SONGS flow velocities are significantly higher than NuScale's uncertainties. The uncertainties in the NuScale hot and cold leg temperatures and flow rates are bounded based on the capabilities of the natural circulation design. Further, the effect of temperature on calculated velocities is low for a subcooled liquid compared to steam conditions.

Steam Generator tube vibrational modes that have a component of cross flow have been evaluated. The SONGS analysis did not consider modes parallel to the anti-vibration bars even though they experience cross flow. Ultimately these were shown to cause FEI. NuScale analyzes all tube frequencies where there is a component of the mode shape in the direction perpendicular to the flow. SONGS bending modes are estimated at approximately 3.7 Hz (Reference 8.21) versus approximately {{ }}$^{2(a),(c),ECI}$ for column 21 of the NuScale SG.

In addition, the SONGS design used a higher damping value of 3% (Reference 8.21). The NuScale analysis uses a more conservative value of 1.5% and this parameter is validated based on testing prior to initial startup testing.

Analysis for FEI is discussed in Section 3.2.1 with results showing positive safety margin. Figure 3-18 demonstrates that the most limiting frequencies and mode shapes of each column, tube and assumed boundary condition in the tube bundle is stable, with a reduced velocity below the low mass damping stability curve. Also included on this figure are the reduced velocity and mass damping for the SONGS replacement steam generator, row 142 and 100, calculated using the same ASME

BPVC Subsection N-1330 equations, but with a less conservative damping value of 3 percent. The SONGS mass damping and reduced velocity values are calculated in Reference 8.21. Depending on the Connors' constants assumed, the predicted safety margin is on the order of negative 830 percent [(8.12-75.67)/8.12] for row 142, using the methodologies of ASME Appendix N.

Figure 3-18 Stability Diagram Results of Asme Appendix N and Chen (Reference 8.22) FEI Test Data with Overlay of NuScale and SONGS Reduced Velocity Values

{{

}}2(a),(c),ECI

3.2.9 Steam Generator Tube Inlet Flow Restrictor Density Wave Oscillation Cavitation Flow Assessment

The loss coefficient for the SG inlet flow restrictors (IFRs) is chosen to preclude density wave oscillation (DWO) from occurring at normal operating power levels of 20 percent and above, and to preclude detrimental effects of DWO at low power conditions. The evaluation of the IFR for turbulent loads for normal operation and under DWO conditions is addressed in Section 3.2.3. This section addresses the effect of cavitation on the IFR and SG tube.

Cavitation occurs when a flowing liquid undergoes a rapid pressure drop to below its vapor pressure causing gas pockets and bubbles to form and collapse at an increased velocity. If the bubble collapse occurs on the surface of a material, the material can erode and possibly reduce the functionality of the geometry where cavitation is occurring. The SG IFRs are a form of restricting orifice where a sudden reduction and expansion in area has the potential to produce cavitation. The SG typically operates in forward, subcooled, stable flow, but below 20 percent power, there is the potential for DWO to occur. The IFR loss coefficient is designed to prevent DWO at higher flows and minimize the adverse effects of DWO at lower flows.

The primary metric to evaluate the propensity of a system to cavitate is the cavitation index. The cavitation index is a dimensionless number comparing the amount of subcooling in the cavitating geometry to the dynamic pressure drop through the restriction:

$$Ca = \frac{P_d - P_v}{\frac{1}{2}\rho v_o^2} \qquad \text{Equation 3-12}$$

where:

Ca = cavitation index (-)

P_d = pressure downstream of orifice (psi)

P_v = vapor pressure at operating conditions (psi)

ρ = fluid density at operating conditions (lb_m/ft^3)

v_o = orifice velocity (ft/s)

Equation 3-12 is reformulated to evaluate the cavitation index at a range of DWO operating conditions:

{{

Equation 3-13

}}2(a),(c),ECI

Incipient cavitation is the onset of cavitation, characterized by light intermittent popping noise. Incipient damage occurs at a lower cavitation number and is the cavitation index at which pitting and erosion begin. For this assessment the cavitation number for onset and damage are conservatively assumed to be equal. The cavitation number for the center-flow IFR is taken from cavitation testing of a center-flow orifice design and scaled to consider dimensional changes between the tested and NPM-20 IFR designs, including the tube area and orifice thickness. Scaling of the incipient cavitation index is conducted using the methodology of Reference 8.25. An orifice with a higher loss is also considered to demonstrate the effect of the loss coefficient on the operational cavitation performance. Results are shown in Table 3-18.

Table 3-18 Center-Holed Orifice Scale Factors and Scaled Incipient Cavitation Index

Center-Holed Orifice Design	Test Incipient Cavitation Index	Tube Flow Area Scaling Factor	Orifice Flow Area Scaling Factor	Orifice Thickness Scaling Factor	Max Scaled Incipient Cavitation Index
{{					
					}}2(a),(c),ECI

Figure 3-19 shows the cavitation index as a function of DWO amplitude for the center-holed orifice IFR design, using varying steady-state conditions as the nominal tube velocity and inlet subcooling consistent with FW plenum enthalpy during steady-state operations. {{

}}2(a),(c),ECI

For two-phase reverse flow, the area contraction from the SG tube into the orifice creates a high velocity, low pressure zone that may increase the vapor fraction of the fluid and increase the length of the vapor cavity, creating slugs of vapor. As this fluid exits the IFR into the FW plenum, the vapor cavities predominantly follow a jetting trajectory out of the IFR, per qualitative analysis of cavitation in thick orifices in Reference 8.24, and collapse in the mostly subcooled liquid contained in the plenum. The erosive damage of cavitation on surfaces is caused by vapor cavities consistently collapsing near the surfaces. The lack of nearby boundaries and surfaces in the FW plenum precludes significant damage due to vapor cavity collapse. This observation is consistent with discussion in Reference 8.25 regarding the use of sudden enlargements to suppress cavitation and erosion damage by removing the boundary from the cavitation zone (Reference 8.25, Section 7.4). Reference 8.25 shows few vapor cavities follow a trajectory that would have the possibility of leading back to the IFR attachment hardware. Further, the IFR attachment hardware is robust, including a tack weld to keep the nut component in place and the IFR inserted into the tube, such that the few vapor cavities that collapse near the hardware do not result in cavitation erosion damage or failure of the IFR attachment.

Figure 3-19 Cavitation Index as a Function of DWO Amplitude for the Center-Hole Orifice IFR during NPM Operations where DWO is Permitted

{{

}}2(a),(c),ECI

The following conclusions can be drawn from Figure 3-19.

- For {{ }}2(a),(c),ECI the nominal tube velocity can be tolerated before cavitation in single-phase liquid flow would occur for any reactor power and FW flow condition. Further analysis below discusses the amount of subcooling that is necessary to preclude cavitation for varying DWO amplitudes.
- The {{

  }}2(a),(c).ECI This is the highest flow condition for single SG operation, so while this is a lower power condition the flow area is smaller, resulting in higher velocities, lower subcooling, and a lower operational cavitation index.

- {{

}}2(a),(c).ECI

- {{

}}2(a),(c),ECI

The previous evaluation assumes that the forward flow through the IFRs during DWO is subcooled to the same level as the FW plenum. In reality, two-phase reverse flow through IFRs during DWO introduces fluid with higher enthalpy than the feedwater flow to the FW plenum such that forward flow through the IFRs during DWO is less subcooled for some portions of the DWO transient. The level of subcooling before cavitation occurs depends on the DWO amplitude. Figure 3-20 and Figure 3-21 provide the minimum subcooling (i.e. maximum inlet enthalpy) that precludes cavitation using nominal conditions from the 10% and 19.99% reactor power operating cases. These figures also show an estimate of the actual mixture enthalpy expected for a bounding range of reverse flow average quality. Inlet conditions during DWO are expected to be closer to the curve assuming average quality consistent with saturated liquid due to subcooled fluid reversing into the plenum for most of DWO operations.

Figure 3-20 Maximum Inlet Enthalpy (Minimum Subcooling) to Preclude Cavitation for 10% Reactor Power, with Mixture Enthalpies for Varying Reverse Flow Average Quality for Context

{{

}}2(a),(c),ECI

Figure 3-21 Maximum Inlet Enthalpy (Minimum Subcooling) to Preclude Cavitation for 19.99% Reactor Power, with Mixture Enthalpies for Varying Reverse Flow Average Qualities for Context

{{

}}2(a),(c),ECI

The only potential operations that could produce cavitation under forward flow conditions are those with low subcooling resulting from very high amplitude DWO and the initial small slug of fluid existing in the IFR at the start of the cycle. This small fraction of a DWO cycle could result in erosion in the SG tubes due to vapor generation in the contraction area section that would then collapse due to partial pressure recovery in the expanded SG tubes. At low power operating conditions with DWO occurring, the amount of DWO operational time it would take to erode through the SG tube wall depends on the transport time of the fluid in the IFR at the start of forward flow. The transport time depends on the mass flow and density of the fluid. Equation 3-14 and Equation 3-15 are used to determine the fraction of DWO period and DWO operational time it would take for the small slugs of high enthalpy fluid to erode through the SG tube wall thickness.

{{

Equation 3-14

Equation 3-15

}}2(a),(c),ECI

Table 3-19 shows this information using the nominal SG tube mass flow rate for reactor powers less than 20 percent.

Table 3-19 DWO Operational Erosion Time for Varying Reactor Powers

Reactor Power (%)	Nominal Tube Mass Flow Rate (lb_m/s)	Velocity (ft/s)	Transport Time (s)	Fraction of DWO Period	DWO Operational Erosion Time	
					hrs	days
{{						
						}}2(a),(c),ECI

Table 3-19 shows that, assuming a consistent DWO period, the lowest reactor powers have a larger fraction of the DWO period when erosion could possibly occur due to the lower mass flow rate and therefore transport time, and therefore would accumulate more erosion over time if the plant is held at those steady state conditions. Apart from low-power testing during startup, extended operational time at these low powers is not expected. For the lowest reactor power evaluated, these highly conservative estimates show it would take {{ }}$^{2(a),(c),ECI}$ to erode through the SG tube due to the small fraction of DWO time where there is the potential to cavitate. Increase in reactor power decreases the fraction of DWO period when cavitation could occur and significantly increases the amount of DWO operational erosion time before SG tube wear-through. The erosion estimates involve several conservative assumptions including:

{{

}}$^{2(a),(c),ECI}$

The above cavitation erosion estimate is for the fraction of forward flow during DWO for which previously reversing flow that is trapped in the IFR is flowing forward through the IFR. It is not expected that the bounding DWO amplitude produces IFR inlet subcooling that causes cavitation in the SG tube during the rest of the forward flow portion of DWO operations.

Erosion evaluations indicate that there is not a concern for significant erosion due to cavitation during DWO. Inspection of the outlet of the IFRs verifies that erosion does not occur at the assumed rates. A sampling of the SG IFR-to-SG tube interfaces is inspected before and after initial startup per Reference 8.13. Startup tests of the NPM, described in FSAR Chapter 14, are performed following the completion of preoperational testing. Startup testing includes initial fuel loading and pre-critical testing, initial criticality testing, low-power testing, and power-ascension testing which provide operating time below 20 percent power. Although cavitation is not expected based on the appropriate sizing of the IFR and the many conservatisms in this evaluation, the planned CVAP inspections confirm whether erosion occurs.

4.0 Vibration Measurement Program

As part of completing the CVAP, experimental testing is conducted to verify the vibration analysis conducted for the NPM. Analysis that shows less than 100 percent safety margin is judged to require verification in the measurement program. Validation testing of novel design changes to preclude FIV, such as flow disrupters, also undergo confirmatory validation testing.

To validate the FIV inputs, analytical results, and the margins of safety determined in the analysis program, a combination of separate effects and initial startup testing are performed. Separate effects testing is performed on a functionally prototypic portion of the steam generator design. Initial startup testing is performed under full-power normal operating conditions. The results of the testing are used to validate the prototype NPM design. Additional details on the measurement program are described in the CVAP Measurement and Inspection Plan Technical Report (Reference 8.13).

5.0 Vibration Inspection Program

Prior to and following initial startup testing, components are inspected for mechanical wear and signs of vibration-induced damage. Additional details for the inspection program are described in the NuScale Comprehensive Vibration Assessment Program Measurement and Inspection Plan Technical Report (Reference 8.13).

6.0 Measurement and Inspection Plan for Non-Prototype NuScale Power Modules

After the CVAP is completed for the first prototype, future NPMs are expected to meet the classification requirements of non-prototype designs. There are no differences between NPMs other than allowable variations in manufacturing tolerances, which are bounded by the validated safety margins for the prototype NPM.

Either a limited vibration measurement program or the prototype inspection program is performed to verify that the vibration analysis and inspection results are consistent with those observed in the prototype NPM. Similar to the approach taken for determining the scope of the prototype measurement program, the results of the prototype measurement and inspection programs are used to inform the required measurement or inspection options for non-prototype NPMs. To ensure that sufficiently bounding and relevant measurements and inspections for non-prototype NPMs are specified, this topic is assessed after the prototype measurement and inspection programs are completed in a separate CVAP report for non-prototype NPMs.

7.0 Summary and Conclusions

To provide assurance that the NPM components do not experience adverse effects of FIV, analysis is performed for NPM components that are susceptible to various FIV mechanisms. The analysis is validated using separate effects and initial startup testing, and component inspections following initial startup testing.

Analysis demonstrates that for all NPM components, FIV is either not predicted to occur or the effects of FIV are shown to be acceptable for the 60-year design life of the module. For components having a safety margin greater than 100 percent for a particular FIV mechanism, testing is not performed. For components with less than 100 percent margin for a particular FIV mechanism, prototype testing is performed to validate key analytical inputs, results and safety margins.

To finalize the CVAP, two additional technical reports are provided. The first report (Reference 8.13) contains the measurement program details for each validation test. The second report provides the post-test evaluation of the testing completed to support the measurement program. In this report, the differences between the expected and measured experimental results are either resolved or confirmed to be in the analytically predicted allowable ranges. The second report contains the inspection program results.

Either a limited vibration measurement program or the prototype inspection program is performed for the non-prototype NPMs to verify the vibration analysis and inspection results are consistent with those observed in the prototype NPM. Similar to the approach taken for determining the scope of the prototype measurement program, the results of the prototype measurement and inspection programs are used to inform the required measurement or inspection options for non-prototype NPMs. To ensure that sufficiently bounding and relevant measurements or inspections for non-prototype NPMs are specified, this topic is assessed after the prototype measurement and inspection programs are completed in a separate CVAP report for non-prototype NPMs.

The CVAP establishes the scope of analyses, testing, measurements, and inspections required to ensure that components of the NPM are not subject to unacceptable vibratory degradation. This report addresses the screening and design analysis aspects of the CVAP. When completed, the CVAP provides the requisite assurance that NPM components are not subject to detrimental effects of FIV.

8.0 Referenced Documents

8.1 American Society of Mechanical Engineers, Boiler and Pressure Vessel Code, 2017 Edition, Section III, Division 1, Appendices, “Appendices-Rules for Construction of Nuclear Facility Components,” New York, NY.

8.2 Au-Yang, M.K., “Flow-Induced Vibration of Power and Process Plant Components, , A Practical Workbook,” American Society of Mechanical Engineers (ASME) Press, New York, NY, 2001.

8.3 Blevins, R.D., Flow-Induced Vibration, Van Nostrand Reinhold, 1990, 2nd Edition.

8.4 Nakamura, Y. and Yoshimura, T., “Flutter and Vortex Excitation of Rectangular Prisms in Pure Torsion in Smooth and Turbulent Flows,” Journal of Sound and Vibration, (1982), Vol. 8, Pages 305 - 317.

8.5 Westinghouse Electric Company, “Advanced Passive 1000 (AP1000) Design Certification Document,” Revision 19, Chapter 4, Chapter 5, Chapter 12, June 2011.

8.6 Mitsubishi Heavy Industries, “Advanced Pressurized-Water Reactor (APWR), Design Certification Document,” Revision 4, Chapter 4, Chapter 5, Chapter 12, September 2013.

8.7 AREVA, “U.S. EPR Design Certification Document,” Revision 5, Chapter 5, Chapter 12, July 2013.

8.8 Electricite de France, “U.K. European Pressurized Reactor, Pre-Construction Safety Report,” Revision 6, Chapter 4,Reactor and Core Design, and Chapter 5, Reactor Coolant System and Associated Systems, October 2012.

8.9 Collins, Elmo E., U.S. Nuclear Regulatory Commission, letter to Peter Dietrich, Southern California Edison Company, July 18, 2012, Agencywide Document Access and Management System (ADAMS) Accession No. ML12188A748.

8.10 ANSYS® Mechanical, Release 19.2, ANSYS, Inc., Canonsburg, PA 2019.

8.11 ANSYS® CFX, Release 19.2, ANSYS, Inc., Canonsburg, PA 2019.

8.12 Chen, S.S., “Flow-Induced Vibration of Circular Cylindrical Structures,” Report No. ANL-85-81, Argonne National Laboratory, Argonne, IL, 1985.

8.13 NuScale Power, LLC, “NuScale Comprehensive Vibration Assessment Program Measurement and Inspection Plan Technical Report,” TR-121354-P.

8.14 Inada, F., “A Study on Leakage-Flow-Induced Vibration From Engineering Viewpoint,” PVP2015-45944, ASME 2015 Pressure Vessels and Piping Conference Volume 4: Fluid-Structure Interaction, July 19-23, 2015, American Society of Mechanical Engineers, New York, NY, 2015.

8.15 Inada, F. and S. Hayama, “A Study on Leakage-Flow-Induced Vibrations. Part 1: Fluid-Dynamic Forces and Moments Acting on the Walls of a Narrow Tapered Passage,” Journal of Fluids and Structures, (1990): 4:395-412.

8.16 Inada, F. and S. Hayama, “A Study on Leakage-Flow-Induced Vibrations. Part 2: Stability Analysis and Experiments for Two-Degree-Of-Freedom Systems Combining Translational and Rotational Motions,” Journal of Fluids and Structures, (1990): 4:413-428.

8.17 Inada, F., “A Parameter Study of Leakage-Flow-Induced Vibrations,” Proceedings of the ASME 2009 Pressure Vessels and Piping Division Conference, July 26-30, 2009, American Society of Mechanical Engineers, New York, NY, 2009.

8.18 Ziada, S & Lafon, Philippe. Flow-Excited Acoustic Resonance Excitation Mechanism, Design Guidelines, and Counter Measures. Applied Mechanics Reviews, Vol. 66, Jan 2014.

8.19 Omer, A., Arafa, N., Mohany, A., & Hassan, M. (2016). The effect of upstream edge geometry on the acoustic resonance excitation in shallow rectangular cavities. International Journal of Aeroacoustics, 15(3), pp. 253-275.

8.20 M. Giraudeau et al. Two-Phase Flow-Induced Forces on Piping in Vertical Upward Flow: Excitation Mechanisms and Correlation Models. Journal of Pressure Vessel Technology, Vol. 135, p. 030907, 2013.

8.21 Blevins, R.D., “Non-Proprietary Application of ASME Code Section III, Appendix N, to SONGS Replacement Steam Generators,” Proceedings of the ASME 2017 Pressure Vessels and Piping Conference, PVP2017-65529, July 2017.

8.22 Chen, S.S., Jendrzejczyk, A., “Experiments on Fluid Elastic Instability in Tube Banks Subjected to Liquid Cross Flow,” Journal of Sound and Vibration 78(3) 355-381, 1981.

8.23 Hobson, D. E., "Fluid-Elastic Instabilities Caused by Flow in Annulus," Proceedings of 3rd International Conference on Vibration in Nuclear Plant, Keswick, pp. 440-463, London: BNES, 1982.

8.24 A. Simpson et al, "Modelling of hydrodynamic cavitation with orifice: Influence of different orifice designs," Chemical Engineering Research and Design, Volume 136, August 2018.

8.25 U.S. Nuclear Regulatory Commission, "Cavitation Guide for Control Valves," NUREG/CR-6031, April 1993.

8.26 P.J. Tygielski et. al. Bellows Flow-Induced Vibrations, NASA Technical Memorandum, NASA TM-82556, October 1983

8.27 American Society of Mechanical Engineers, Boiler and Pressure Vessel Code, 2017 Edition, Section III Subsection NG, “Core Support Structures”, New York, NY.